

# Nonperturbative quantum field theory for pseudo-Goldstone modes, slow-Goldstone modes, and their quantum chaos

Fadi Sun and Jinwu Ye

*School of Sciences, Great Bay University, Dongguan 523000, China;*

*Great Bay Institute for Advanced Study, Great Bay University, Dongguan 523808, China;*

*and Dongguan Key Laboratory for Quantum Black Hole and Quantum*

*Error Correction, Great Bay University, Dongguan 523000, China*

(Dated: August 21, 2025)

In this work, we develop a novel form of non-perturbative theory to identify a light pseudo-Goldstone mode with a small mass, as well as a new type of Goldstone mode with a tiny slope (termed the slow-Goldstone mode), which may not be obtained via traditional perturbative methods. We demonstrate our formalism in the context of superfluids formed by Rashba spin-orbit coupled spinor bosons in a square lattice weakly interacting with a spin-anisotropic interaction. The experimental detections of these two modes, especially their roles leading to the quantum information scramblings at a finite temperature are discussed. The slow-Goldstone mode is compared with the slow light and the soft mode in the Sachdev-Ye-Kitaev models. This non-perturbative formalism can be widely applied to study other emergent particles in various quantum matter.

## I. INTRODUCTION

Quantum field theory usually is studied by a perturbative expansion in terms of a small parameter such as the fine structure constant in QED, or quark-gluon coupling in the short distance scale due to the asymptotic freedom in QCD [1]. However, when studying some strong coupling problems such as the strong CP violation problem, conventional perturbation theory fails, a new non-perturbative method needs to be developed. This fact motivates various techniques in quantum field theory and string theory to reach non-perturbative results from asymptotic series in some coupling constants with zero radius of convergence [2–4]. Similar difficulties may also appear when studying low energy emergent quantum phenomena in quantum matters. Indeed, when evaluating various experimentally measurable quantities in quantum materials, one usually apply some popular perturbative expansion in terms of a small parameter such as  $1/N$  expansion in quantum magnets [5, 6] and Sachdev-Ye-Kitaev model [7–9], or  $1/S$  expansion in quantum magnets [10] or a weak interaction in the superfluids [11].

In particular, retaining only a few lowest order terms in perturbative expansions may fail to capture fundamental physics and generate spurious results that violate exact symmetry constraints. Our work investigates superfluid phases of Rashba spin-orbit-coupled spinor bosons in a square lattice system with weak spin-anisotropic on-site interactions. This system provides a concrete manifestation of such limitations: naive perturbative treatments yield unphysical gapless excitations where symmetry arguments strictly require gapped modes, or produce Goldstone modes with erroneous dispersion relations that contradict symmetry-breaking predictions. Previous approaches incorporating the order from quantum disorder (OFQD) analysis[10] – a mechanism that incorporates quantum fluctuations to lift accidental degeneracies – fails to cure these spurious results. These drawbacks motivated us to develop a new non-perturbative formal-

ism to completely remove these spurious results and lead to new important physical results consistent with exact symmetry arguments. In sharp contrast to the results achieved by the various resurgent method in math [2] and high-energy physics [3, 4], these results on the emergent phenomena in quantum matters can be directly measured in the current experiments of cold atoms loaded in optical lattices.

The Rashba or Dresselhaus spin-orbit coupling (SOC) is ubiquitous in various 2d or layered non-centrosymmetric insulators [12, 13], semi-conductor systems [14, 15], metals [16], and superconductors [17]. The lattice regularization of a linear combination of the Rashba and Dresselhaus SOC,  $\alpha k_x \sigma_x + \beta k_y \sigma_y$ , corresponds to the kinetic energy of the system. The SOC anisotropy can be adjusted by strain, surface geometry, or applied gate electric fields. In the cold-atom experiments, there were experimental advances to generate 2d Rashba SOC for the fermionic  $^{40}\text{K}$  gas [18, 19] and the tunable quantum anomalous Hall (QAH) SOC for bosonic  $^{87}\text{Rb}$  atoms in a square lattice [20]. More recently, the optical lattice clock scheme has been implemented to generate very long lifetime 1d SOC for various atoms [21–27]. The 2d Rashba SOC with a long enough lifetime in a square lattice maybe generated in some near future cold-atom experiments.

A strongly interacting Rashba SOC spinor bosons at integer fillings in a square lattice was studied in [28] in the Mott insulating phase. In this work, we investigate various spin-bond correlated superfluids of the same model in the weak interaction limit at arbitrary fillings. Focus is placed on the anisotropic SOC ( $\alpha = \pi/2, \beta$ ) with a spin-anisotropic interaction parameter  $\lambda$ . Due to the heating issue[20], the small  $\beta$  regime ( $0 < \beta < \beta_c \approx 0.29\pi$ ) is experimentally more accessible. In this regime, the analysis is highly dependent on the parameter  $\lambda$ , leading to three distinct phases:

For  $\lambda < 1$ , we identify a classical degenerate family of ground states due to a spurious  $U(1)$  symme-

try. The first-step OFQD analysis [10] which lifts spurious degeneracies through zero-point energy corrections, identifies the plane-wave with spin polarization along  $x$ -direction (PW-X) superfluid (SF) phase [29] as the quantum ground state. This phase features two (gapless) linear modes: the superfluid Goldstone mode at the momentum  $(0, 0)$  due to  $U(1)_c$  symmetry breaking, and a roton mode at the momentum  $(\pi, 0)$  due to the spurious  $U(1)$  symmetry [30]. Applying the second-step OFQD method developed in [10], we find that the roton mode acquires a small gap with a gap exponent  $\nu = 1/2$ , thus transformed into a pseudo-Goldstone mode (see Fig.4(a)) [31].

At  $\lambda = 1$ , the superfluid Goldstone mode remains uncritical, but the roton mode becomes a spurious quadratic one, again due to the spurious  $U(1)$  symmetry. Unfortunately, the conventional second-step OFQD method [10] fails to resolve these issues, prompting the development of a new approach that successfully determines the entire spectrum. This new scheme successfully transforms the roton mode into a SOC Goldstone mode with a linear dispersion, dictated by the  $U(1)_{\text{soc}}$  symmetry breaking at  $\lambda = 1$ . A notable feature of this SOC Goldstone mode is its near-flat dispersion, resulting in slower propagation compared to the superfluid Goldstone mode -hence the name “slow-Goldstone mode” (see Fig.4(b)). As a by-product, our scheme also determines the full spectrum of the pseudo-Goldstone mode for  $\lambda < 1$ , beyond its gap at zero momentum reached in [10]. We analyze the novel quantum information scrambling due to both modes, and find that the pseudo-Goldstone mode ( $\lambda < 1$ ) leads to exponential suppression of the Lyapunov exponent, while the slow-Goldstone mode ( $\lambda = 1$ ) leads to  $T^3$  scaling of the Lyapunov exponent; see Table I.

For  $\lambda > 1$ , a classical analysis identifies the ground state is a superfluid phase with spin polarized along  $Z$ -direction and exhibiting sign alternation between adjacent sites along the  $x$ -direction. This phase is referred to as the  $Z$ -x SF phase. A conventional perturbative calculation in the  $Z$ -x SF phase opens a gap to the slow-Goldstone mode at  $\lambda = 1$  with the gap exponent  $\nu = 1$ , as shown in Fig. 4(c). Thus, the mechanism generates distinct critical correlation exponents on either side of the quantum critical point, driven by roton softening and the near-flat slow-Goldstone mode at  $\lambda = 1$ . A comparison is drawn between the slow-Goldstone mode and the superfluid Goldstone mode regarding their distinct Kosterlitz-Thouless (KT) transitions: the former drives a spin-orbit KT transition at  $T_{\text{KT}}^{\text{soc}}$ , while the latter governs a superfluid KT transition at higher  $T_{\text{KT}}^{\text{SF}}$ . Our method may also be extended to explore other emergent particles in many other quantum materials.

The paper is organized as follows. In Sec. II, we define the Hamiltonian, analyze its exact symmetries. In Sec. III, we perform a mean-field analysis, and identify the relevant spurious symmetries. Section IV investigates quantum ground states and emergent Goldstone modes across the three regimes ( $\lambda < 1$ ,  $\lambda = 1$ ,  $\lambda > 1$ ). Finite-

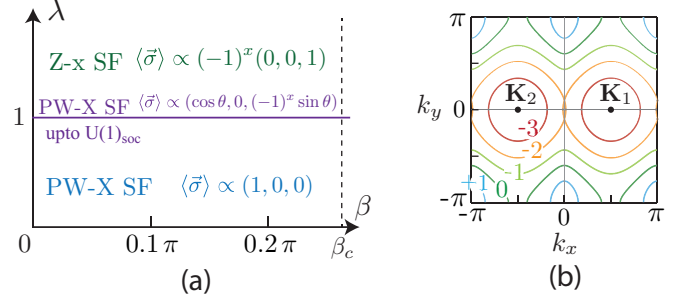


FIG. 1. (a) Quantum phase diagram in the  $(\beta, \lambda)$  plane along the anisotropic SOC line ( $\alpha = \pi/2, \beta$ ), in the weak interaction limit. The system remains in a superfluid phase throughout. A  $U(1)_{\text{soc}}$  symmetry is present at  $\lambda = 1$ , but is explicitly broken at the spin-dependent interaction  $\lambda \neq 1$ . (b) Contour plot of the non-interacting spectrum  $\epsilon_-(\mathbf{k})$  for fixed  $\beta = \pi/10$ . There are  $N_K = 2$  minima of  $\epsilon_-(\mathbf{k})/t$  at  $\mathbf{K}_{1,2} = (\pm\pi/2, 0)$  in the experimentally accessible regime  $0 < \beta < \beta_c \approx 0.29\pi$  [32].

temperature phase transitions, quantum chaos behaviors, and experimental detection schemes are presented in Sec. V. Section VI provides a comparative analysis: contrasting the slow-Goldstone mode with slow-light phenomena and soft modes in Sachdev-Ye-Kitaev models. Some technical details are provided in four Appendices.

## II. THE INTERACTING SOC MODEL AND EXACT SYMMETRIES

We study spinor bosons with short-range interactions hopping in a square lattice subject to a non-Abelian gauge field [28]:

$$\mathcal{H} = -t \sum_{\langle i,j \rangle} \sum_{\sigma\sigma'} (b_{i\sigma}^\dagger U_{ij}^{\sigma\sigma'} b_{j\sigma'} + h.c.) + \frac{U}{2} \sum_i (n_{i\uparrow}^2 + n_{i\downarrow}^2 + 2\lambda n_{i\uparrow} n_{i\downarrow}) - \mu \sum_{i,\sigma} n_{i\sigma}, \quad (1)$$

where  $b_{i\sigma}$  ( $b_{i\sigma}^\dagger$ ) annihilates (creates) a boson with spin  $\sigma = \{\uparrow, \downarrow\}$  at site  $i$ ,  $n_{i\sigma} = b_{i\sigma}^\dagger b_{i\sigma}$  is the number operator,  $\langle i, j \rangle$  denotes nearest-neighbor pairs,  $t$  is the hopping amplitude,  $U$  ( $\lambda U$ ) parametrizes the intra-spin (inter-spin) repulsive interaction, and  $\mu$  is the chemical potential.  $U_{i,i+\hat{x}} = e^{i\alpha\sigma_x}$  and  $U_{i,i+\hat{y}} = e^{i\beta\sigma_y}$  are the non-Abelian gauge potentials put on the two links in the square lattice. Setting  $\alpha = \beta = 0$ , Eq.(1) reduces to the conventional pseudospin-1/2 (two-component) Bose-Hubbard model. This work focuses on various novel superfluids phases arising from anisotropic SOC ( $\alpha = \pi/2$  and  $0 < \beta < \beta_c \approx 0.29\pi$ ) and spin-anisotropic interaction  $\lambda$ . The quantum phase diagram is shown in Fig.1(a).

In the weak interaction limit  $U \ll t$ , one can first diagonalize the hopping term, and then treat the interaction  $U$  as a small perturbation, leading to an asymptotic expansion series. For fixed  $\alpha = \pi/2$  and

and  $0 \leq \beta < \beta_c$ , the hopping part in momentum space is:  $\mathcal{H}_0 = -2t \sum_{\mathbf{k}} b_{\mathbf{k}}^\dagger [\cos \beta \cos k_y - \sin k_x \sigma_x - \sin \beta \sin k_y \sigma_y] b_{\mathbf{k}}$ . The two eigen-energies takes the form:  $\epsilon_{\pm}(\mathbf{k}) = -2t(\cos \beta \cos k_y \mp \sqrt{\sin^2 k_x + \sin^2 \beta \sin^2 k_y})$ . As shown in Fig.1(b),  $\epsilon_{-}(\mathbf{k})$  develops  $N_K = 2$  minima at  $\mathbf{k} = (\pm\pi/2, 0)$ , and the corresponding eigenspinors are  $(1, \mp 1)^T / \sqrt{2}$ , respectively. Note that the eigenspinors are independent of the SOC parameter  $\beta$ , which may cause a spurious symmetry arise from the higher symmetry case at  $\beta = 0$ .

To analyze the exact symmetries of the model, we define the spin operators as  $S_i^a = \sum_{\sigma\sigma'} b_{i\sigma}^\dagger \sigma_{\sigma\sigma'}^a b_{i\sigma'}$ , where  $a = x, y, z$ . In the special limit  $\lambda = 1$  and  $\beta = 0$ , the non-Abelian gauge field on the  $x$ -links can be gauged away through the transformation  $b_j \rightarrow \exp(-i\alpha j_x \sigma_x) b_j$ . This transformation reveals a hidden spin-orbital coupled  $SU(2)$  symmetry generated by:  $Q_X = \sum_i S_i^x$ ,  $Q_Y = \sum_i (-1)^{i_x} S_i^y$ , and  $Q_Z = \sum_i (-1)^{i_x} S_i^z$ . Derivations from  $\lambda = 1$  and  $\beta = 0$  break this symmetry in different ways: For  $\lambda = 1$  and  $\beta \neq 0$ , only  $Q_Y$  commutes with the  $\mathcal{H}$ , reducing the symmetry to a spin-orbital coupled  $U(1)_{\text{soc}}$ ; for  $\lambda \neq 1$  and  $\beta = 0$ , only  $Q_Z$  remains conserved; for  $\lambda \neq 1$  and  $\beta \neq 0$ , all three generators are explicitly broken. In addition to these spin-related symmetries, the model always preserves the global charge  $U(1)_c$  symmetry generated by particle number conservation  $\sum_{i,\sigma} n_{i,\sigma}$ . Furthermore, the Hamiltonian  $\mathcal{H}$  respects several discrete  $Z_2$  reflection symmetry: (1)  $\mathcal{P}_x$ :  $k_y \rightarrow -k_y, S_i^y \rightarrow -S_i^y, S_i^x \rightarrow S_i^x, S_i^z \rightarrow -S_i^z$ . (2)  $\mathcal{P}_y$ :  $k_x \rightarrow -k_x, S_i^x \rightarrow -S_i^x, S_i^y \rightarrow S_i^y, S_i^z \rightarrow -S_i^z$ . (3)  $\mathcal{P}_z$ :  $k_x \rightarrow -k_x, S_i^x \rightarrow -S_i^x, k_y \rightarrow -k_y, S_i^y \rightarrow -S_i^y, S_i^z \rightarrow S_i^z$ . This  $\mathcal{P}_z$  symmetry is also equivalent to a joint  $\pi$  rotation of orbital and spin around  $\hat{z}$  axis.

### III. MEAN-FIELD ANALYSIS AND ORIGIN OF SPURIOUS SYMMETRIES

At  $0 < \beta < \beta_c$ , the lower band develops  $N_K = 2$  minima at momenta  $(\pm\pi/2, 0)$  see Fig.1(b). In the weak interaction regime, most of the bosons condense into the single-particle state, which is superposition of the eigenstates at the two degenerate minima of the lower band. The single-particle wave-function takes the form

$$\Psi_i^0 = \frac{1}{\sqrt{2N_s}} \left[ c_1 e^{i\mathbf{K} \cdot \mathbf{r}_i} \begin{pmatrix} 1 \\ -1 \end{pmatrix} + c_2 e^{-i\mathbf{K} \cdot \mathbf{r}_i} \begin{pmatrix} 1 \\ 1 \end{pmatrix} \right], \quad (2)$$

where  $\mathbf{K} = (\pi/2, 0)$ ,  $N_s$  is the total number of lattice sites, and  $c_{1,2}$  are complex coefficients satisfying the normalization condition subject to the normalization condition  $|c_1|^2 + |c_2|^2 = 1$ .

By construction, the mean-field kinetic energy is independent of  $c_{1,2}$ . The total energy minimization therefore reduces to minimizing the interaction energy alone. For general  $\lambda$ , the mean-field interaction energy density is:

$$E_{\text{int}}^0 = \frac{U n_0^2}{2} \left( 1 + \frac{\lambda - 1}{2} [1 - (c_1 c_2^* + c_1^* c_2)^2] \right), \quad (3)$$

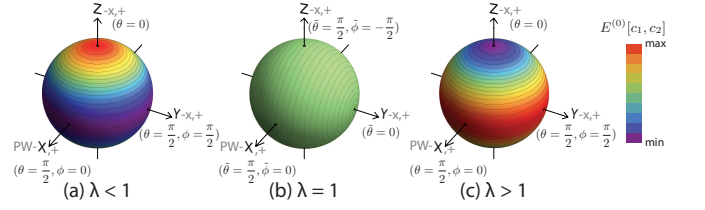


FIG. 2. Contour plots of the *classical* ground-state energy  $E^{(0)}[c_1, c_2]$  on the Bloch sphere (constrained by  $|c_1|^2 + |c_2|^2 = 1$  modulo a global  $U(1)$  phase). (a) For  $\lambda < 1$ , minima of  $E^{(0)}$  occur along the equator. This spurious degeneracy will be lifted by quantum corrections. (b) For  $\lambda = 1$ ,  $E^{(0)}$  remains constant over the entire sphere. The  $U(1)_{\text{soc}}$  symmetry preserves exact degeneracy along meridians (dashed lines) for arbitrary  $\phi$  at fixed  $\theta$ , while quantum corrections will select a specific  $\tilde{\theta}$ . (c) For  $\lambda > 1$ , minima of  $E^{(0)}$  localize at north/south pole (Z-x states).

where  $N_0$  is the number of condensed atom, and  $n_0 = N_0/N_s$  is the condensate density. Minimization of  $E_{\text{int}}^0$  with respect to  $c_{1,2}$  yields distinct mean-field ground states.

When  $\lambda = 1$ , the mean-field interaction energy Eq.(3) is independent of  $c_{1,2}$ . When  $\lambda < 1$ , its minima are reached when  $|c_1 c_2^* + c_1^* c_2|$  is minimized, that is  $c_1 c_2^* + c_1^* c_2 = 0$ . When  $\lambda > 1$ , its minima are reached when  $|c_1 c_2^* + c_1^* c_2|$  is maximized, that is  $c_1 c_2^* + c_1^* c_2 = \pm 1$ . The naive parameterization  $c_1 = e^{+i\phi/2} \cos(\theta/2)$  and  $c_2 = e^{-i\phi/2} \sin(\theta/2)$  lead to  $c_1 c_2^* + c_1^* c_2 = \cos \phi \sin \theta$ . For  $\lambda < 1$  this enforces  $\cos \phi \sin \theta = 0$ , i.e.  $\phi = \pm\pi/2$  with arbitrary  $\theta$ . However, this parameterization becomes singular at the plane-wave solution — namely  $\theta = 0$  (where  $c_2 = 0$ ) and  $\theta = \pi$  (where  $c_1 = 0$ ) — leaving  $\phi$  undefined and preventing a unified treatment of the accidental degeneracy. To resolve these singularities, it is convenient to introduce two Z-x states, which satisfy  $Q_Z \Psi_{Z-x,\pm}^0 = \pm \Psi_{Z-x,\pm}^0$ :

$$\Psi_{Z-x,\pm}^0 = \frac{1}{2\sqrt{N_s}} \left[ e^{i\mathbf{K} \cdot \mathbf{r}_i} \begin{pmatrix} 1 \\ -1 \end{pmatrix} \pm e^{-i\mathbf{K} \cdot \mathbf{r}_i} \begin{pmatrix} 1 \\ 1 \end{pmatrix} \right], \quad (4)$$

which can be called Z-x basis. This basis can be used to re-parameterize Eq.(2) as:

$$\Psi_i^0 = e^{i\phi/2} \cos(\theta/2) \Psi_{Z-x,+}^0 + e^{-i\phi/2} \sin(\theta/2) \Psi_{Z-x,-}^0, \quad (5)$$

which means that in Eq.(2):

$$\begin{aligned} c_1 &= [e^{i\phi/2} \cos(\theta/2) + e^{-i\phi/2} \sin(\theta/2)] / \sqrt{2}, \\ c_2 &= [e^{i\phi/2} \cos(\theta/2) - e^{-i\phi/2} \sin(\theta/2)] / \sqrt{2}, \end{aligned} \quad (6)$$

and the interaction energy simplifies to

$$E_{\text{int}}^0 = \frac{U n_0^2}{2} \left( 1 + \frac{\lambda - 1}{2} \sin^2 \theta \right), \quad (7)$$

which is explicitly independent of the angle  $\phi$  (see Fig.2).

As discussed in Sec. 3, turning on a nonzero  $\beta$  reduces the exact symmetry: for  $\lambda = 1$ ,  $\beta > 0$  reduces the  $SU(2)$

to exact  $U(1)_{\text{soc}}$  ( $Q_Y$  conserved); for  $\lambda \neq 1$ ,  $\beta > 0$  explicitly breaks  $Q_Y$  conservation, leaving no continuous spin symmetry. Nonetheless, since Eq.(3) is independent of  $\beta$ , the classical ground-state manifold may exhibit an accidental degeneracy arising from spurious symmetry. Specifically, for  $\lambda = 1$  and  $\beta > 0$ , the classic ground-state manifold is the (two dimensional) sphere, whereas the exact symmetry  $U(1)_{\text{soc}}$  is only one-dimensional. This extra degeneracy stems from a spurious  $U(1)$  symmetry inherited from the original  $SU(2)$  at  $\beta = 0$ . When  $\lambda < 1$  and  $\beta > 0$ , the classic ground-state manifold is the (one dimensional) equator of sphere. Since there is no exact continuous spin symmetry, the continuous degeneracy is due to a spurious  $U(1)$  symmetry inherited from the exact  $U(1)$  symmetry at  $\beta = 0$ . When  $\lambda > 1$ , the classic ground-state manifold is north/south pole of sphere, thus the ground-state degeneracy is due to spontaneous breaking of the exact symmetry  $\mathcal{P}_z$  and no spurious  $U(1)$  symmetry anymore.

#### IV. QUANTUM GROUND STATE AND VARIOUS GOLDSTONE MODES

We have determined the classical ground state, which exhibits accidental degeneracy due to spurious symmetry. As will be demonstrated, this spurious symmetry generates unphysical artifacts — not only in ground-state degeneracy but also in low-energy excitations. These spurious results will be cured through systematic inclusion of quantum fluctuations within the quantum order from disorder (OFQD) framework. The OFQD procedure comprises two steps: the first step is correcting the ground state energy and identifying the quantum ground state; the second step is correcting the low-energy excitations and obtaining Goldstone modes respecting exact symmetry constraints.

To begin our analysis, we first review the standard perturbative method for bosonic atoms in optical lattices [33]. In the weak interaction regime, the spinor field can be decomposed into a condensate and fluctuation components:  $b = \sqrt{N_0}\Psi_0 + \psi$ , where  $N_0$  is the number of condensate atoms and  $\psi$  are bosonic quantum fluctuation fields. Substituting this decomposition into the Hamiltonian yields an asymptotic expansion:

$$\mathcal{H} = \mathcal{H}^{(0)} + \mathcal{H}^{(1)} + \mathcal{H}^{(2)} + \dots, \quad (8)$$

where the superscript denotes the order in the fluctuations  $\psi$  and  $\dots$  means higher-order terms. The leading term  $\mathcal{H}^{(0)} = E^{(0)}$  gives the classical ground-state energy. Setting  $\mathcal{H}^{(1)} = 0$  determines the chemical potential. Diagonalizing  $\mathcal{H}^{(2)}$  through a Bogoliubov transformation  $(\psi, \psi^\dagger) \rightarrow (\beta, \beta^\dagger)$  that preserves canonical bosonic commutation relations yields:

$$\mathcal{H}^{(2)} = E_0^{(2)} + \sum_{\mathbf{k}} \sum_l \omega_l(\mathbf{k}) \left( \beta_{l,\mathbf{k}}^\dagger \beta_{l,\mathbf{k}} + \frac{1}{2} \right), \quad (9)$$

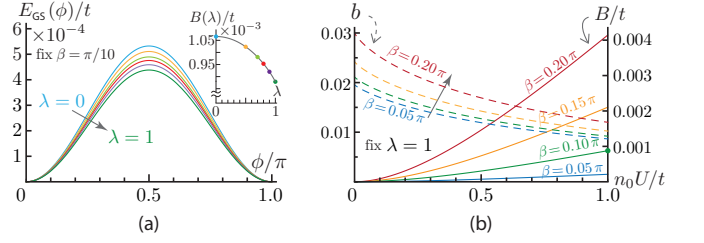


FIG. 3. (a) The quantum corrected ground state energy as a function of  $\phi$  at fixed  $\beta = \pi/10$  and  $n_0U/t = 1$ , for various  $\lambda = 0, 0.5, 0.7, 0.8, 0.9, 1.0$ . The  $\phi$  variation corresponds to equatorial trajectories on the Bloch sphere in Fig. 2. The insert shows the extracted value for  $B$  as a function of  $\lambda$ . (b)  $B(\lambda = 1)$  and  $b = Bt/(n_0^2 U^2 \sin^2 \beta)$  as a function of  $n_0U/t$  for various  $\beta = 0.05\pi, 0.10\pi, 0.15\pi, 0.20\pi$ .

where  $\omega_l(\mathbf{k})$  are Bogoliubov excitation energy bands. These represent the dispersion relations of collective modes in the system, with  $l$  indexing distinct excitation branches. The zero-point energy contribution yields the quantum corrected ground-state energy:

$$E_{\text{GS}} = E_{0t} + \frac{1}{2} \sum_{\mathbf{k}} \sum_l \omega_l(\mathbf{k}), \quad (10)$$

with  $E_{0t} = E^{(0)} + E_0^{(2)}$ . While this approach is valid without spurious symmetries, special care is required when accidental degeneracies exist. In the following sections, we study  $\lambda < 1$ ,  $\lambda = 1$ , and  $\lambda > 1$  in detail.

##### A. PW-X SF at $\lambda < 1$ and pseudo-Goldstone mode

For  $\lambda < 1$ , minimization of the classical ground-state energy Eq.(7) fixes  $\theta = \pi/2$  but leaves  $\phi$  undetermined. This results in a large number of accidental degenerated ground-state due to the spurious  $U(1)$  symmetry. To resolve this degeneracy, we perform an OFQD analysis to study quantum corrections to the ground-state energy.

Setting  $\theta = \pi/2$  in  $\Psi_i^0$  yields a wave-function that depends on  $\phi$ , denoted  $\Psi_i^0(\phi)$ . Decomposing the spinor field as  $b_i = \sqrt{N_0}\Psi_i^0(\phi) + \psi$ , generates the asymptotic expansion  $\mathcal{H} = \mathcal{H}^{(0)} + \mathcal{H}^{(1)} + \mathcal{H}^{(2)}(\phi) + \dots$ , where the classic ground-state energy  $\mathcal{H}^{(0)}$  is  $\phi$ -independent,  $\mathcal{H}^{(1)} = 0$  determines the value of the chemical potential  $\mu = -2t(1 + \cos \beta) + Un_0(1 + \lambda)/2$ , and  $\mathcal{H}^{(2)}$  exhibits explicit  $\phi$ -dependence. Diagonalizing  $\mathcal{H}^{(2)}$  through an  $8 \times 8$  Bogoliubov transformation yields four  $\phi$ -dependence Bogoliubov bands  $\omega_l(\mathbf{k}; \phi)$  ( $l = 1, 2, 3, 4$ ). Consequently, the quantum corrected ground-state energy become  $\phi$ -dependent. Numerical evaluation of  $E_{\text{GS}}(\phi)$  via Eq. (10) in Fig. 3 reveals minima at  $\phi = 0, \pi$ . So the “quantum order from disorder” mechanism selects  $\phi = 0$  corresponds  $(c_1, c_2) = (1, 0)$ , or  $\phi = \pi$  corresponds  $(c_1, c_2) = (0, 1)$ , among the classical degenerate family tuned by  $\phi$ . Both configurations correspond to spin polarization along the  $X$ -direction, establishing the plane-wave- $X$  superfluid



(PW-X SF) phase. Besides, these states exhibit opposite spin orientations along  $X$  and spontaneously break the discrete  $\mathcal{P}_y$  and  $\mathcal{P}_z$  symmetries.

### 1. Superfluid Goldstone Mode and Spurious Linear Mode

Having established the PW-X SF state as the quantum ground state, we now analyze its excitation spectrum and critical behavior in the limits  $\lambda \rightarrow 1^-$  and  $\beta \rightarrow 0^+$ .

Examining the low-energy properties of the lowest Bogoliubov band  $\omega_1(k)$ , we find two gapless linear modes located at momenta  $(0, 0)$  and  $(\pi, 0)$ , respectively. Expansion around these momenta gives

$$\begin{aligned}\omega_G(\mathbf{q}) &= \sqrt{n_0 t U (1 + \lambda) [q_x^2 + u(\beta) q_y^2]}, \\ \omega_R(\mathbf{q}) &= \sqrt{n_0 t U (1 - \lambda) [q_x^2 + u(\beta) q_y^2]},\end{aligned}\quad (11)$$

where  $u(\beta) = \cos \beta - \sin^2 \beta$ , with momentum measured relative to  $(0, 0)$  and  $(\pi, 0)$ . The first mode,  $\omega_G$ , is the expected superfluid Goldstone mode resulting from spontaneous  $U_c(1)$  symmetry breaking. The second mode,  $\omega_R$ , is the roton mode, exhibits spurious linear dispersion. As we demonstrate below,  $\omega_R$  will acquire a small gap through the OFQD mechanism, and transformed into a pseudo-Goldstone mode.

In the following, we will perform the second-step OFQD analysis first developed in [10] on the roton mode.

### 2. Pseudo-Goldstone Mode from OFQD Mechanism

Combining the classical energy Eq.(7) and quantum-corrected energy Eq.(10), we can extract the  $\theta$  and  $\phi$  dependence of the ground-state energy around its minimum:

$$\mathcal{H} = E_{0t} + \frac{1}{2} A (\delta\theta)^2 + \frac{1}{2} B (\delta\phi)^2, \quad (12)$$

where  $\theta = \pi/2 + \delta\theta$  and  $\phi = 0 + \delta\phi$ . The coefficient  $A = \partial^2 E_{int}^0 / \partial \theta^2|_{\theta=\pi/2} = (1 - \lambda) U n_0^2 / 2$  originates from the classical contribution, which is extracted from Eq.(7), while  $B(\lambda) = \partial^2 E_{GS} / \partial \phi^2|_{\phi=0} = b(n_0 U \sin \beta)^2 / t$  comes from the quantum contribution which can be numerically determined from Fig.3(a).

Since  $n_0 \delta\theta/2$  and  $\delta\phi$  form conjugate variables satisfying  $[n_0 \delta\theta/2, \delta\phi] = i\hbar$ , the second-step OFQD mechanism generates the roton gap [10]:

$$\Delta_R^- = 2\sqrt{AB}/n_0 \sim n_0 U \sqrt{(1 - \lambda)U/t}. \quad (13)$$

Obviously, the non-analytic behaviours in both the SOC parameter  $\lambda$  and the weak interaction  $U$  can only be achieved from the second-step non-perturbative OFQD mechanism.

As demonstrated below, the  $B$  term in Eq.(12) remains non-critical as  $\lambda$  approaches  $1^-$ . There is a 2nd order

quantum phase transition (QPT) from the PW-X to the Z-x phase induced by the roton dropping as  $\lambda \rightarrow 1^-$ , so the quantum critical behaviour of the roton gap  $\Delta_R^- \propto \sqrt{1 - \lambda}$  when  $\lambda < 1$  (See also Fig.4(a)).

Unfortunately, the second-step OFQD mechanism developed in [10] can only achieve the roton gap at  $(\pi, 0)$  instead of the whole excitation spectrum. This shortcoming can only be overcome by the new method developed here. The technical details are presented in the two appendices from both canonical quantization and the path integral approach. The final answer is to change the roton mode in Eq.(11) to

$$\omega_R(\mathbf{q}) = \sqrt{\Delta_R^2 + B_R [q_x^2 + (\cos \beta - C \sin^2 \beta) q_y^2]}, \quad (14)$$

where  $\Delta_R = \omega_R(\mathbf{q} = 0) = \sqrt{2BU(1 - \lambda)}$  is the roton gap in Eq.(13) generated by the second-step OFQD mechanism already developed in [10]. So our unified scheme recovers the previously developed OFQD at the zero momentum, but went much beyond.

### 3. Spurious Gapless Quadratic Mode as $\lambda \rightarrow 1^-$

As  $\lambda \rightarrow 1^-$ , the superfluid Goldstone mode remains un-critical, but the roton mode in Eq.(11) becomes a quadratic one:

$$\omega_R^0(\mathbf{q}) = t \sqrt{[q_x^2 + u(\beta) q_y^2][q_x^2 + v(\beta) q_y^2]}, \quad (15)$$

where  $v(\beta) = \cos \beta - \frac{\sin^2 \beta}{1 + n_0 U / 2t} > u(\beta)$ .

This quadratic dispersion is spurious and can be viewed as the remanent of the ferromagnetic mode due to the  $\tilde{S}U_s(2)$  symmetry breaking at the Abelian point ( $\alpha = \pi/2, \beta = 0$ ). In fact, this problem has already been cured in Eq.(14); setting  $\lambda = 1$  turns the spurious quadratic mode into the linear SOC Goldstone mode in Eq.(23). In the following section, we take a different basis to show that it will be turned into a linear SOC Goldstone mode with a tiny slope at  $\lambda = 1$  through the newly developed mechanism.

## B. PW-X SF at $\lambda = 1$ and slow-Goldstone mode

When  $\lambda = 1$  and  $\beta < \beta_c$ , Eq.(3) shows that any  $c_1$  and  $c_2$  give the same interaction energy, thus they form a classically degenerate ground-state manifold due to the spurious  $SU(2)$  symmetry originated from the exact  $\tilde{S}U(2)_s$  symmetry stressed in the Sec.2.

It was known [28] that the Hamiltonian Eq.(1) at  $\alpha = \pi/2$  and  $\lambda = 1$  has a spin-orbit coupled  $U_{\text{soc}}(1)$  symmetry  $Q_Y = \sum_i (-1)^{i_x} S_i^y$ . In order to distinguish between an accidental degeneracy and the exact degeneracy, we introduce two Y-x states:

$$\Psi_{Y-x, \pm}^0 = \frac{1}{2\sqrt{N_s}} \left[ e^{i\mathbf{K} \cdot \mathbf{r}_i} \begin{pmatrix} 1 \\ -1 \end{pmatrix} \pm i e^{-i\mathbf{K} \cdot \mathbf{r}_i} \begin{pmatrix} 1 \\ 1 \end{pmatrix} \right], \quad (16)$$

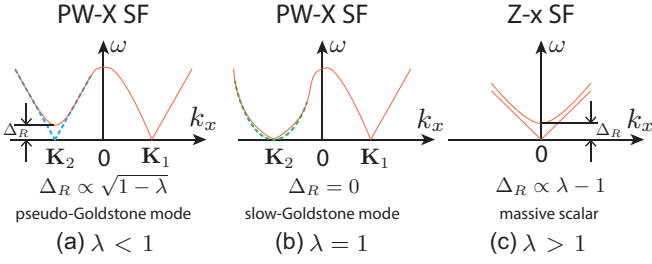


FIG. 4. Evolution of the low energy excitations as  $\lambda$  changes from  $\lambda < 1$  to  $\lambda = 1$  and  $\lambda > 1$  at a fixed  $0 < \beta < \beta_c$ . (a) The tiny roton gap  $\Delta_R^- \sim \sqrt{1-\lambda}$  generated by non-perturbative quantum corrections at  $\lambda < 1$ . Its non-analytic behaviour can only be captured by the non-perturbative approach. The conventional perturbative calculations would lead to the spurious linear mode (dashed line). (b) The slow-Goldstone mode at  $\mathbf{K}_2 = (-\pi/2, 0)$  due to the  $U(1)_{\text{soc}}$  breaking generated by non-perturbative quantum corrections at  $\lambda = 1$ . Its slope is much smaller than that of the superfluid Goldstone mode at  $\mathbf{K}_1 = (\pi/2, 0)$ . The conventional perturbative calculations would lead to the spurious quadratic mode (dashed line). (c) The large roton gap  $\Delta_R^+ \sim \lambda - 1$  in the Z-x SF state at  $\lambda > 1$ . Its analytic behaviour can be reached simply by a perturbative calculation. The superfluid Goldstone mode at  $(\pi/2, 0)$  from the  $U(1)_c$  breaking remains uncritical through the transition.

which satisfy  $Q_Y \Psi_{Y-x, \pm}^0 = \pm \Psi_{Y-x, \pm}^0$ . It can be called the Y-x basis (see Fig.2(b)), in contrast to the Z-x basis (see Fig.2(a)) listed below Eq.(4). In fact, the two basis are dual to each other under the exchange of variables in Eq.(21).

It can be used to re-parameterize Eq.(2) as:

$$\Psi_i^0 = e^{i\tilde{\phi}/2} \cos(\tilde{\theta}/2) \Psi_{Y-x, +}^0 + e^{-i\tilde{\phi}/2} \sin(\tilde{\theta}/2) \Psi_{Y-x, -}^0, \quad (17)$$

which means that in Eq.(2):

$$\begin{aligned} c_1 &= [e^{i\tilde{\phi}/2} \cos(\tilde{\theta}/2) + e^{-i\tilde{\phi}/2} \sin(\tilde{\theta}/2)]/\sqrt{2}, \\ c_2 &= i[e^{i\tilde{\phi}/2} \cos(\tilde{\theta}/2) - e^{-i\tilde{\phi}/2} \sin(\tilde{\theta}/2)]/\sqrt{2}, \end{aligned} \quad (18)$$

which differs from Eq.(6) just by an extra “i” in  $c_2$  due to the extra “i” in Eq.(16).

The  $U(1)_{\text{soc}}$  symmetry at  $\lambda = 1$  dictates that the energy should be independent of  $\phi$ . We expect that the classical degeneracy at the angle  $\theta$  will be lifted by quantum effects, and a unique  $\theta$  will be determined by the OFQD mechanism (see Fig.2(b)).

We set  $\phi = 0$  to spontaneously breaks the  $U(1)_{\text{soc}}$  symmetry. Following the similar procedures as in the Sec. IV A, we obtain Eqs.(9),(10) which picks up its minima at  $\theta = \pi/2$ . So the OFQD mechanism still selects the PW-X state ( $\theta = \pi/2, \phi = 0$ ). All the other exactly degenerate states can be generated by changing  $\phi$ . If we take  $c_1 = 1, c_2 = 0$  PW-X state in Eq.(2), then the  $U(1)_{\text{soc}}$  related family is

$$\Psi_i^0 = \frac{1}{\sqrt{2N_s}} \left[ \cos \frac{\tilde{\phi}}{2} e^{i\mathbf{K} \cdot \mathbf{r}_i} \begin{pmatrix} 1 \\ -1 \end{pmatrix} - \sin \frac{\tilde{\phi}}{2} e^{-i\mathbf{K} \cdot \mathbf{r}_i} \begin{pmatrix} 1 \\ 1 \end{pmatrix} \right], \quad (19)$$

whose corresponding spin-orbital structure is

$$S_i^x = -\cos \tilde{\phi}, \quad S_i^y = 0, \quad S_i^z = -(-1)^x \sin \tilde{\phi}. \quad (20)$$

Setting  $\tilde{\phi} = 0, \pi$  and  $\tilde{\phi} = \pi/2, 3\pi/2$  recovers the two PW-X states and the Z-x,  $\pm$  states, respectively (see Fig.2).

By comparing  $\lambda < 1$  state  $\Psi_i^0(\theta = \pi/2, \phi)$  in Eq.(5) with  $\lambda = 1$  state  $\Psi_i^0(\tilde{\theta}, \tilde{\phi} = 0)$  in Eq.(17) we can see the relation between the sets of the OFQD variables in the two cases:

$$\tilde{\theta} = \pi/2 - \phi, \quad (21)$$

which just shows the  $(\theta, \phi)$  exchanges in the Z-x basis in Eq.(4) and the Y-x basis in (16). As claimed below Eq.(16), the two basis are dual to each other (Fig.2).

### 1. Failure of Conventional OFQD Analysis in [10]

The  $U_{\text{soc}}(1)$  symmetry dictates no  $\phi$  dependence, so the ground-state energy can be written as:

$$E_{GS}(\theta) = E_{GS}(\theta = \pi/2) + \frac{1}{2}B(\delta\theta)^2 \quad (22)$$

where  $\delta\theta = \theta - \pi/2$  and  $B = B(\lambda = 1)$  can be extracted from Fig.3. The classical  $A$  term in Eq.(12) vanishes as dictated by the exact  $U_{\text{soc}}(1)$  symmetry. Because  $\lim_{\lambda \rightarrow 1} B(\lambda < 1) = B(\lambda = 1)$ , so  $B(\lambda)$  is continuous at  $\lambda = 1$ . Unfortunately, plugging  $A = 0$  into Eq.(13) still leads to  $\Delta_R^- = 0$ , so the conventional 2nd-step non-perturbative OFQD analysis developed in [10] can not lead to any useful information in this case. One must develop a more advanced non-perturbative method which can not only evaluate the gap at  $q = 0$ , but also the whole spectrum in the long wavelength limit. This lofty goal was achieved here by developing a non-perturbative method. The technical details are presented in the two appendices from both canonical quantization and the path integral approach.

### 2. Slow-Goldstone Mode via Newly Developed non-perturbative Approach

As shown in the Appendixes A and B, the newly developed non-perturbative method successfully changes the spurious quadratic dispersion of the roton mode in Eq.(15) to a linear one which is nothing but the SOC Goldstone mode due to the spontaneous breaking of the  $U_{\text{soc}}(1)$  symmetry,

$$\omega_R(q) = \sqrt{\frac{2Bt}{n_0}} [q_x^2 + v(\beta)q_y^2] \quad (23)$$

where because  $B = b(n_0 U \sin \beta)^2/t$ , so the slope of the SOC Goldstone mode  $v_{\text{soc}} \sim \sqrt{n_0}U$  is much softer than the superfluid velocity  $c \sim \sqrt{n_0}Ut$  of the superfluid

Goldstone mode in Eq.(11) (see Fig.4(b)). The ratio  $r_G = v_{soc}/c$  between the slope of Goldstone mode and superfluid Goldstone mode is plotted in Fig.5b. So the SOC Goldstone mode travels much slower than that of the superfluid Goldstone mode. Due to the wide momentum separation between the superfluid Goldstone and the roton mode, the superfluid Goldstone mode is not affected by the non-perturbative analysis.

### C. Z-x SF at $\lambda > 1$ and perturbative calculation

When  $\lambda > 1$  and  $\beta < \beta_c$ , the minimization of Eq.(3) requires  $c_1 c_2^* + c_1^* c_2 = \pm 1$  which means  $c_1 = \pm c_2 = e^{i\gamma}/\sqrt{2}$  where  $\gamma$  is a globe phase. So the two-fold degenerated ground state is either  $\Psi_{Z-x,+}$  with  $c_1 = c_2 = 1/\sqrt{2}$  or  $\Psi_{Z-x,-}$  with  $c_1 = -c_2 = 1/\sqrt{2}$  (see Fig.2(c)). So the ground state is determined at the mean-field level upto the exact symmetry  $\mathcal{P}_z$ .

Let us pick up the  $\Psi_{Z-x,+}$  state, we find its 4 excitation modes  $\omega_{1,2,3,4}(\mathbf{k})$  in ascending order:  $\omega_1(\mathbf{k})$  contains a Goldstone mode at  $(0,0)$ ,  $\omega_2(\mathbf{k})$  contains a roton mode at  $(0,0)$  (see Fig.4(c)) and  $\omega_{3,4}(\mathbf{k})$  are high-energy bands (not shown in Fig.4(c)). Note that the Z-x SF state breaks the translation symmetry to two sites per unit cell, so the Brillouin zone (BZ) in the Z-x state becomes the Reduced BZ (RBZ) with  $-\pi/2 < k_x < \pi/2$ ,  $-\pi < k_y < \pi$  shown in Fig.4(c).

When  $\lambda > 1$ , one can extract the long wave length limit of superfluid Goldstone mode  $\omega_1$  and the roton mode  $\omega_2$ :

$$\begin{aligned} \omega_1(\mathbf{k}) &= \sqrt{2n_0 t U [k_x^2 + w(\beta, \lambda) k_y^2]}, \\ \omega_2(\mathbf{k}) &= (\lambda - 1)n_0 U + t[k_x^2 + x(\beta, \lambda) k_y^2], \end{aligned} \quad (24)$$

where

$$\begin{aligned} w(\beta, \lambda) &= \cos \beta - \frac{\sin^2 \beta}{1 + (\lambda - 1)n_0 U / 4t}, \\ x(\beta, \lambda) &= \cos \beta - \frac{4t(4t + \lambda n_0 U) \sin^2 \beta}{16t^2 + 8tn_0 U - n_0^2 U^2 (\lambda - 1)^2}, \end{aligned} \quad (25)$$

and  $\mathbf{k} \in RBZ$ . Because  $w(\beta, \lambda = 1) = u(\beta)$  listed below Eq.(11), it recovers the superfluid Goldstone mode in Eq.(11) at  $\lambda = 1$ . Note that  $(\lambda - 1)U \ll t$ , so despite the minus sign in the denominator of  $x(\beta, \lambda)$ , there is no divergency in it.

In contrast to the pseudo-Goldstone mode Eq.(14), the roton mode is non-relativistic with the roton gap:

$$\Delta_R^+ = \omega_2(0, 0) = (\lambda - 1)n_0 U \quad (26)$$

which, in contrast to Eq.(13), is analytic in both  $\lambda$  and  $n_0 U$  as shown in Fig.3(c). When one gets very close to the QCP such that  $|\lambda - 1| < U/t \ll 1$ , the gap is smaller than that in the Pseudo-Goldstone mode side. When one gets far away from the QCP such that  $|\lambda - 1| > U/t$ , the gap is larger than that in the Pseudo-Goldstone mode side.

## V. FINITE TEMPERATURE BEHAVIOURS AND EXPERIMENTAL DETECTIONS

In the previous sections, we examined the pseudo-Goldstone mode and the slow-Goldstone mode through the non-perturbative approach developed in this work. While these modes are only the elementary excitations of the interacting SOC system. At finite temperature, particularly in the vicinity of the QPT driven by the spin-anisotropy interaction  $\lambda$ , as illustrated in Fig.5(a), it becomes essential to investigate the many-body behaviors that go beyond, yet remain complementary to, the elementary excitations. A salient feature of interacting systems near a QPT at finite temperature is the emergence of quantum chaotic dynamics, which will be the focus of this section. Furthermore, we will elucidate the intrinsic connections between the quantum chaotic properties of the system and those associated with its elementary excitations, as summarized in Table I.

### A. Finite temperature phase transitions and quantum chaos

Now we briefly discuss the finite temperature phases and phase transitions above all the SFs in Fig. 1. Of course, due to the spontaneous  $U(1)_c$  symmetry breaking in all the superfluid phases at  $T = 0$ , there is always a KT transition  $T_{KT}^{SF}$  above all the superfluids. At  $\lambda = 1$ , due to the spontaneous  $U(1)_{soc}$  symmetry breaking at  $T = 0$ , there is also a KT transition  $T_{KT}^{soc}$  in Figs.5. Due to the correlated spin-bond orders of the SFs, there are also other interesting phase transitions associated with

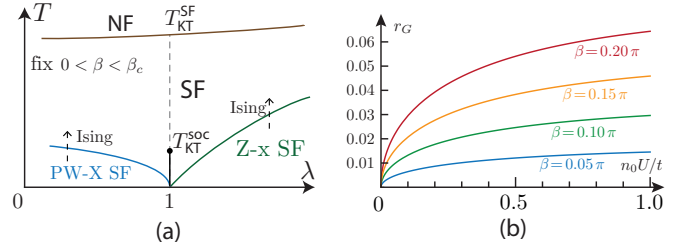


FIG. 5. The finite temperature phase transitions and Quantum chaos driven by the roton touchdown corresponding to Fig.4. (a) At  $\lambda = 1$ , there is a Kosterlitz–Thouless (KT) transition at  $T_{KT}^{soc}$  due to the slow-Goldstone mode in the SOC sector. There is always a higher KT transition at  $T_{KT}^{SF}$  from the superfluid to a normal fluid (NF) due to the SF Goldstone mode in the density sector. There is a Ising melting transition in the PW-X SF and Z-x SF restoring the discrete  $\mathcal{P}_y$  symmetry, respectively. The transition temperature  $T_2 \sim \Delta_R \sim |\lambda - 1|^\nu$  where  $\nu = 1/2, 1$  scales as the roton gap at  $(-\pi/2, 0)$  in Fig.4. At  $\lambda = 1$ , the two states become degenerate due to the  $U(1)_{soc}$  symmetry. (b) The ratio between the slope of slow-Goldstone mode and superfluid Goldstone mode as a function of  $n_0 U/t$  at  $\lambda = 1$  (see Appendix D). The typical value for  $r_G$  is  $\sim 1\%$ .

the restorations of these spin-bond correlated orders at a finite temperature shown in Fig.5. The nature of these finite temperature transitions can be qualitatively determined by the degeneracy of the ground states: PW-X ( $d = 2$ ), Z-x SF ( $d = 2$ ) which breaks  $\mathcal{P}_y$  (also  $\mathcal{P}_z$ ) and  $\mathcal{P}_y$  (also  $\mathcal{P}_x$ ), respectively.

Taking two initially commuting operators separated by a large spatial distance  $x$ ,  $[W(x, 0), V(0, 0)] = 0$ , and assuming  $\langle V \rangle_\beta = \langle W \rangle_\beta = 0$ , one can study how the commutator evolves over time under the Hamiltonian  $H$ :

$$C(x, t) = \langle [W(x, t), V(0, 0)]_\pm^\dagger [W(x, t), V(0, 0)]_\pm \rangle_\beta, \quad (27)$$

where  $W(x, t) = e^{iHt}W(x, 0)e^{-iHt}$  and the  $\pm$  applies when  $W$  and  $V$  are fermionic and bosonic operators respectively. The average  $\langle \dots \rangle_\beta$  could be the infinite temperature  $\beta = 0$  or any finite temperature.

For a quantum chaotic system, the quantum information scrambling encoded in  $C(x, t)$  can be described by:

$$C(x, t) = f_0 - f_1 e^{\lambda_L(t - |x|/v_B)} \quad (28)$$

where  $\lambda_L$  is the Lyapunov exponent,  $v_B$  is the butterfly velocity. The physical picture is the following: under a quantum chaotic evolution, the operator  $W(x, t)$  will grow ballistically with a characteristic quantum butterfly velocity  $v_B$ . The  $W(x, t)$  and  $V(0, 0)$  still commute, so  $C(x, t)$  remains small, until a scrambling time  $t_s > |x|/v_B$  when  $V(0, 0)$  enters the butterfly light cone of  $W(x, t)$ . So it is the ballistic growth of the commutators in the spatial directions which defines the butterfly light-cone  $|x| = v_B t$  around which the quantum information scrambling increases exponentially with the Lyapunov exponent  $\lambda_L$  in Eq.(28). The butterfly velocity  $v_B$ , in general, should satisfy the Lieb-Robinson bound on the commutator of local operators separated in time for systems with local interactions [34], so  $v_B$  may also be called Lieb-Robinson velocity. In the present context,  $W = V$  can be chosen as the density or spin operator of the system. Then it represents the quantum information scramblings in the density and spin channel respectively.

(1) *Enhanced Quantum information scramblings due to the SOC Goldstone mode*

One usually classify quantum chaos as the following 5 classes in terms of the Lyapunov exponent  $\lambda_L$  at a low temperature  $T$ : (i) maximal quantum chaos  $\lambda_L = 2\pi T/\hbar$ , (ii) quantum chaos  $\lambda_L \sim aT$  where  $a < 2\pi/\hbar$ , (iii) weak quantum chaos  $\lambda_L \sim T^b$  where  $b > 1$ , (iv) suppressed quantum chaos  $\lambda_L \sim e^{-T/\Delta}$  where  $\Delta$  is the gap of the system, and finally (v) an integrable system  $\lambda_L = 0$ .

It is the gap which determines the Lyapunov exponent  $\lambda_L$ , while it is the dispersion which determines the butterfly velocity  $v_B$  with the corresponding light cone  $x - v_B t$  (Table I). Because the superfluid (or density) sector is non-critical, so we only focus on the roton (or SOC) sector in Fig.5. It is important to point out that the "QPT" driven by the spin-anisotropy interaction  $\lambda$  in Fig.5 is different than the conventional one: there is an exact  $U(1)_{soc}$  symmetry at  $\lambda = 1$ , so in contrast to

the enlarged emergent symmetry due to the spontaneous symmetry breaking where there is an enhanced quantum chaos  $\lambda_L \sim aT$  where  $a < 2\pi/\hbar$  (for example, the quantum Lifshitz transition driven by the superfluid Goldstone boson at  $\beta = \beta_c$  in Fig.1 to be mentioned in the conclusion), here it is the exact symmetry, so it is just has a weak quantum chaos  $\lambda_{L,R} \sim T^3/\rho_{s,R}^2$  where  $\rho_{s,R}$  is the superfluid density in the SOC sector which, as computed in the Appendix B, is much smaller than that in the superfluid sector, so the coefficient in the front of  $T^3$  becomes quite large. The corresponding butterfly velocity  $v_{B,R} = v_{soc} \sim \sqrt{n_0}U$  listed below Eq.(23) is also very tiny as shown in Fig.5(b). When  $\lambda \neq 1$ , a gap is opened with  $\Delta_R \sim |1 - \lambda|^\nu$  where  $\nu = 1/2, 1$  listed in Eq.(13) and Eq.(26) respectively, so the quantum chaos is exponentially suppressed with  $\lambda_{L,R} \sim e^{-T/\Delta_R}$ . The corresponding butterfly velocity is given by  $v_{B,Rx} = \sqrt{\frac{B_R}{\Delta_R}}T$  if  $T \ll \Delta_R$  or  $v_{B,Rx} = \sqrt{B_R}$  if  $T > \Delta_R$  in Eq.(14) and  $V_{B,Rx} = \sqrt{tT}$  if  $T \ll \Delta_R$  in Eq.(24). These facts may also be considered as the enhancement of quantum chaos at the "QPT" driven by the spin-anisotropy interaction  $\lambda$  in Fig.5(a).

## B. Detections in cold-atom experiments

The pseudo-spin-1/2 boson can be experimentally realized using ultracold alkaline atoms. For example, in  $^{87}\text{Rb}$  ( $5S_{1/2}$ ), nuclear spin  $I = 3/2$  leads to an  $F = 1$  electronic ground state. One can choose with hyper-fine state  $|\uparrow\rangle = |F = 1, m_F = -1\rangle$  and  $|\downarrow\rangle = |F = 1, m_F = 0\rangle$ , while the third state  $|F = 1, m_F = +1\rangle$  can be removed by a sufficiently large two-photon detuning[20]. As suggested in [35], SOC may be realized in near future experiments by adding spin-flip Raman lasers or by driving the spin-flip transition with radio-frequency or microwave fields. Due to the heating issues associated with the SOC generated by Raman laser scheme on alkali fermions, it would be difficult to observe many body phenomena on alkali fermions with the Raman scheme [18, 19]. However, optical lattice clock schemes [23] have been successfully implemented to generate SOC for  $^{87}\text{Sr}$  [25] and  $^{173}\text{Yb}$  [24]. This newly developed scheme has the advantage to suppress the heating issue suffered in the Raman scheme. It can also probe the interplay between the interactions and the SOC easily.

The time of flight (TOF) image after a time  $t$  is given by [36]:

$$n(\mathbf{r}) = (M/\hbar t)^3 f(\mathbf{k}) G(\mathbf{k}), \quad (29)$$

where  $\mathbf{k} = M\mathbf{r}/\hbar t$ ,  $f(\mathbf{k}) = |w(\mathbf{r})|^2$  is the form factor due to the Wannier state of the lowest Bloch band of the optical lattice and  $G(\mathbf{k}) = \frac{1}{N_s} \sum_{i,j} e^{-\mathbf{k} \cdot (\mathbf{r}_i - \mathbf{r}_j)} \langle \Psi_i^\dagger \Psi_j \rangle$  is the equal time boson structure factor. For small condensate depletion in the weak interaction limit  $U/t \ll 1$ ,  $\langle \Psi_i^\dagger \Psi_j \rangle \sim \langle \Psi_{0i}^\dagger \Psi_{0j} \rangle$  where  $\Psi_{0i}^\dagger$  is the condensate wavefunction Eq.(2) at the mean field level. So the TOF can



TABLE I. The quantum information scrambling behaviours of the pseudo-Goldstone mode and the slow-Goldstone mode achieved by the non-perturbative approach developed here.  $\Delta_R^- \sim \sqrt{1-\lambda}$ ,  $\Delta_R^+ \sim \lambda - 1$ . The massive scalar at  $\lambda > 1$  can be reached just by perturbation theory and is listed here only for completeness and comparison.

Deformation	Particle	Spurious	Corrected	Lyapunov exponent	Butterfly velocity
$\lambda < 1$	pseudo-Goldstone	$\omega \sim k$	$\omega \sim \sqrt{(\Delta_R^-)^2 + v^2 k^2}$	$\lambda_L \sim e^{-\Delta_R^-/T}$	$v_B \sim v\sqrt{T/\Delta_R^-}$ , $T \ll \Delta_R^-$
$\lambda = 1$	slow-Goldstone	$\omega \sim k^2$	$\omega \sim v_{soc} k$	$\lambda_L \sim T^3/\rho_{s,R}^2$	$v_B \sim v_{soc} \ll c$
$\lambda > 1$	massive scalar	—	$\omega \sim \Delta_R^+ + tk^2$	$\lambda_L \sim e^{-\Delta_R^+/T}$	$v_B \sim \sqrt{T}t$ , $T \ll \Delta_R^+$

detect the quantum ground state wavefunction such as the PW-X and Z-x state in Fig.4 directly.

The anisotropic interaction  $\lambda$  in Eq.(1) can be easily tuned between two species of spinor bosons in two different hyperfine states. All the superfluid phases, their excitation spectrum and the transition driven by a tiny gapped pseudo-Goldstone mode touch down at  $\lambda < 1$  to become the soft SOC Goldstone mode at  $\lambda = 1$ , then a large gapped pseudo-Goldstone mode at  $\lambda > 1$  shown in Fig.4 can be precisely determined by various experimental techniques such as dynamic or elastic, energy or momentum resolved, longitudinal or transverse-Bragg spectroscopies [37–41], specific heat measurements [42, 43] and *In-Situ* measurements [44]. The very narrow butterfly light-cone  $x - v_{B,R}t$  along the time direction due to the Goldstone boson in the SOC sector can also be detected by the techniques developed in [45, 46].

## VI. DISCUSSION

There are two kinds of Goldstone modes in the SOC interacting system studied here. One is the superfluid Goldstone mode due to the  $U(1)_c$  symmetry breaking. Its velocity can be easily calculated just by the conventional perturbative method. Another is the slow-Goldstone mode at  $\lambda = 1$  due to the  $U(1)_{soc}$  breaking. Its tiny velocity can only be computed by the new non-perturbative formalism developed here. The two Goldstone modes play very different roles, especially in displaying quantum information scramblings in terms of Lyapunov exponent and butterfly velocity (see Table I). This slow-Goldstone may be contrasted to the slow light [47] which is the propagation of an optical pulse or other modulation of an optical carrier at a very low group velocity. Of course, complete different mechanisms are responsible for the slowness of the spin-0 and spin-1 bosons respectively. The former is due to the spurious symmetry at the classical level and the non-perturbative OFQD mechanism developed in this work. The latter occurs when a propagating pulse is substantially slowed by the interaction with the medium in which the propagation takes place.

It is also interesting to contrast the pseudo-Goldstone and Goldstone mode discovered here by the formalism here with the soft Goldstone mode identified by  $1/N$  ex-

pansion in the Sachdev-Ye-Kitaev (SYK) models. In the SYK models [7–9, 48], the saddle point solution spontaneously breaks the reparametrization symmetry to the global  $SL(2, Z)$  symmetry, resulting a zero Goldstone mode. Then when considering the leading irrelevant operator  $-i\omega$  perturbatively in the  $1/N$  expansion which also breaks the reparametrization symmetry explicitly, it will lift the zero Goldstone mode to a gapless (soft) Pseudo-Goldstone mode described by the Schwartzian, which leads to the maximal quantum chaos. So in the SYK case, a leading order in  $1/N$  expansion is enough to capture the main physics of SYK models: the maximal chaos which is dual to that of a quantum black hole. There is no need for any non-perturbative formalism to capture the soft pseudo-Goldstone mode. Due to the lack of the space dimension in the SYK model, there is no dispersion relation for such a soft mode, also no associated butterfly velocity. As stressed in the Sec.V, in the present interacting SOC system, there are the intrinsic connections between the quantum chaotic properties of the system and those of the elementary excitations as listed in the Table I. It is the slow-Goldstone mode at  $\lambda = 1$  which leads to the enhanced quantum chaos characterized by the power law Lyapunov exponent and a very slow butterfly velocity. It is also the small gap  $\Delta_R^-$  of the pseudo-Goldstone mode at  $\lambda < 1$  which leads to the suppressed quantum chaos characterized by the exponentially suppressed Lyapunov exponent and a power law vanishing butterfly velocity at a low temperature  $T \ll \Delta_R^-$ .

Here we develop a new and systematic non-perturbative approach to investigate this new class of QPT induced by the roton touchdown at  $\lambda = 1$  leading to the slow-Goldstone mode. The superfluid Goldstone mode remains un-critical through such a process. The quantum Lifshitz transition induced by the superfluid Goldstone mode at  $\beta = \beta_c$  in Fig.1 will be addressed elsewhere. As shown in [28], at integer fillings and  $\lambda = 1$ , the system described by Eq.(1) enters the Mott insulating Y-x phase in the strong coupling limit ( $U/t \gg 1$ ). We note that the Y-x superfluid phase shown in Fig. 2, which occurs in the weak coupling limit ( $U/t \ll 1$ ), shares the same spin-orbital structure as this Mott insulating phase. It is therefore interesting to investigate potential quantum and topological phase transitions between these states. Such transitions may occur through inter-

mediate quantum spin liquid phases as increasing  $U/t$ , connecting the Y-x superfluid phase (with both superfluid Goldstone and slow-Goldstone bosons) to the Y-x Mott phase. The non-perturbative approach developed here could be widely used to study novel emergent quantum phenomena in many other frustrated systems, also in particle physics related to the Coleman-Weinberg effective potential [49]. Additionally, our formalism might exhibit superficial similarities to the resurgent theory developed in topological strings and matrix models, though establishing any rigorous connections requires further investigation.

## ACKNOWLEDGMENTS

We thank Jing Zhou for helpful discussions. This work is supported by Guangdong Basic and Applied Basic Research Foundation (Grant No. 2024A1515010698).

*Note added.*— After we finished this work, a new experiment [50] appeared, it realized a tunable  $SU(2)$  gauge field of spinor bosons of  $^{87}\text{Rb}$  atoms loaded in a one dimensional ladder system.

## Appendix A: Canonical quantization approach to capture the non-perturbative effect

In this appendix, a unified non-perturbative scheme is developed to compute the whole excitation spectrum, extending well beyond the gap-calculation scheme in [10] and containing it at the zero momentum point. This approach automatically includes not only the mass generation of the pseudo-Goldstone mode at  $\lambda < 1$ , but also the computation of the spectrum of the slow-Goldstone mode at  $\lambda = 1$ .

We perform our non-perturbative analysis using the Z-x representation Eq. (4), though equivalent results may be obtained in the dual Y-x representation Eq. (16), which is related to the Z-x basis by the duality transformation in Eq. (21) and is employed in Sec. IV (see Fig. 2). Since  $B(\lambda)$  in Eq. (12) and Eq. (22) is continuous at  $\lambda = 1$  as shown in Fig. 3(a), we only need focus on the  $\lambda < 1$  case and then take the  $\lambda \rightarrow 1^-$  limit. We need to establish the relation between the OFQD variables  $\phi$  in Eq. (12) in the old OFQD analysis and the original Bose fields in Eq. (1).

The Bose condensation Eq. (2) inspires us to parameterize the most general Bose field in the polar-like coordinate system as

$$\Psi_i = e^{i\chi} \sqrt{\rho} [c_1 \eta_1 e^{i\mathbf{K} \cdot \mathbf{r}_i} + c_2 \eta_2 e^{-i\mathbf{K} \cdot \mathbf{r}_i}] , \quad (\text{A1})$$

where one can parameterize the two coefficients  $c_{1,2}$  in the most general forms in the Z-x representation in Eq. (6) and the two-component spinors  $\eta_{1,2}$  as:

$$\eta_n = \begin{pmatrix} e^{+i\phi_n/2} \cos(\theta_n/2) \\ e^{-i\phi_n/2} \sin(\theta_n/2) \end{pmatrix}, \quad n = 1, 2. \quad (\text{A2})$$

Thus we can write  $\Psi_i = \Psi_i(\rho, \chi, \theta, \phi, \theta_1, \phi_1, \theta_2, \phi_2)$ , which also takes into account the quantum fluctuations of the two spinors  $\eta_{1,2}$ .

Since we already found the quantum ground state is the PW-X SF state which corresponds to the saddle point values:

$$\Psi_{i,0} = \Psi_i(\rho_0, 0, \pi/2, 0, -\pi/2, 0, \pi/2, 0). \quad (\text{A3})$$

One can write down the quantum fluctuations around the saddle point as  $\Psi_i = \Psi_{i,0} + \delta\Psi_i$ , where  $\delta\Psi_i$  can be expressed as a function of  $\delta\rho, \chi, \delta\theta, \phi, \delta\theta_1, \phi_1, \delta\theta_2, \phi_2$ . Thus, we can separate the Bose field into the condensation part plus the quantum fluctuation part in the polar coordinate system:

$$\begin{aligned} \Psi_i &= \sqrt{\frac{\rho_0}{2}} \begin{pmatrix} 1 \\ -1 \end{pmatrix} e^{i\mathbf{K} \cdot \mathbf{r}_i} \\ &+ \sqrt{\frac{\rho_0}{8}} \left[ \left( \frac{\delta\rho}{\rho_0} + i\chi \right) \begin{pmatrix} 1 \\ -1 \end{pmatrix} + (\delta\theta_1 + i\phi_1) \begin{pmatrix} 1 \\ 1 \end{pmatrix} \right] e^{i\mathbf{K} \cdot \mathbf{r}_i} \\ &+ \sqrt{\frac{\rho_0}{8}} (-\delta\theta + i\phi) \begin{pmatrix} 1 \\ 1 \end{pmatrix} e^{-i\mathbf{K} \cdot \mathbf{r}_i}, \end{aligned} \quad (\text{A4})$$

where the third line explicitly contains the OFQD variable  $\phi$ .

On the other hand, in the original Cartesian coordinate, we have:

$$\Psi_i = \sqrt{\frac{N_0}{2}} \begin{pmatrix} 1 \\ -1 \end{pmatrix} e^{i\mathbf{K} \cdot \mathbf{r}_i} + \begin{pmatrix} \psi_{i\uparrow} \\ \psi_{i\downarrow} \end{pmatrix}, \quad (\text{A5})$$

After comparing both the  $e^{i\mathbf{K} \cdot \mathbf{r}_i}$  and the  $e^{-i\mathbf{K} \cdot \mathbf{r}_i}$  components in the two equations Eq. (A4) and Eq. (A5), one can express the OFQD variable  $\phi$  in terms of the original Bose field. After a Fourier transformation this leads to

$$\phi_{\mathbf{q}} = \frac{-i}{\sqrt{2\rho_0}} [\psi_{-\mathbf{K}+\mathbf{q},\uparrow} + \psi_{-\mathbf{K}+\mathbf{q},\downarrow} - \psi_{\mathbf{K}-\mathbf{q},\uparrow}^\dagger - \psi_{\mathbf{K}-\mathbf{q},\downarrow}^\dagger], \quad (\text{A6})$$

where, as expected, only the quantum fluctuations near  $-\mathbf{K}$  appear in the relation. Thus we can express the quantum correction coming from the OFQD mechanism in terms of the original Bose fields as:

$$\delta\mathcal{H} = \sum_i \frac{B}{2} \phi_i^2 = \sum_q \frac{B}{2} \phi_q \phi_{-q}, \quad (\text{A7})$$

which, we must stress, only holds in the momentum regime near  $-\mathbf{K}$ , so it will not affect the Goldstone mode near  $\mathbf{K}$ .

Finally, after combining with  $\mathcal{H}^{(2)}$  in Eq. (9) (its expression before applying the Bogoliubov transformation, see Appendix C), we arrive at the non-perturbative Hamiltonian:

$$\mathcal{H} = \mathcal{H}^{(2)} + \delta\mathcal{H} = \frac{1}{2} \sum_q \Psi_q^\dagger (M + \delta M) \Psi_q, \quad (\text{A8})$$

where the  $4 \times 4$  matrix  $M$  was already obtained from the PW-X SF calculation leading to Eq.(9), and the matrix  $\delta M$  can be written in a  $4 \times 4$  matrix form:

$$\delta M = \frac{B}{2n_0} \begin{pmatrix} 1 & 1 & -1 & -1 \\ 1 & 1 & -1 & -1 \\ -1 & -1 & 1 & 1 \\ -1 & -1 & 1 & 1 \end{pmatrix}. \quad (\text{A9})$$

We diagonalize the Hamiltonian Eq.(A8) by a  $4 \times 4$  Bogoliubov transformation:

$$\mathcal{H} = \sum_{l=1}^2 \sum_{q \in BZ} \omega_l(\mathbf{q}) \left( \beta_{l,q}^\dagger \beta_{l,q} + \frac{1}{2} \right), \quad (\text{A10})$$

where  $\omega_1(\mathbf{q}) \leq \omega_2(\mathbf{q})$ . Thus one only needs to focus on the lowest band  $\omega_1$ . Note that here we started from the PW-X SF state in Eq.(A3), so  $\mathbf{q}$  is defined in the whole Brillouin zone, in contrast to the OFQD analysis Eq.(10) where  $\mathbf{k}$  defines in the reduced Brillouin zone.

From the complete form of the dispersion  $\omega_1(-\mathbf{K} + \mathbf{q})$ , we can extract the long wavelength limit of the Pseudo-Goldstone mode as listed in Eq.(14)

$$\omega_R(\mathbf{q}) = \sqrt{\Delta_R^2 + B_R[q_x^2 + (\cos \beta - C \sin \beta)q_y^2]}, \quad (\text{A11})$$

where  $\Delta_R = \omega_R(\mathbf{q} = 0) = \sqrt{2BU(1-\lambda)}$  is the roton gap in Eq.(13) generated by the 2nd step OFQD mechanism already developed in [10]. So our unified scheme recovers the previously developed OFQD at the zero momentum, but goes much further. The two coefficients  $B_R = 2Bt/n_0 + n_0Ut(1-\lambda)$  and  $C = 1 + \frac{BU[4t(1-3\lambda)+2B(1-\lambda)/n_0+n_0U(1-\lambda)^2]}{[2B/n_0+n_0U(1-\lambda)][8t^2+2n_0Ut(1+\lambda)-BU(1-\lambda)]} < 1$  represent the corrections to the roton dispersion, which can only be achieved by the new non-perturbative formalism developed here. These terms are important and lead to the butterfly velocity of the pseudo-Goldstone mode:  $v_{B,Rx} = \sqrt{(B_R/\Delta_R)T}$  if  $T \ll \Delta_R$  or  $v_{B,Rx} = \sqrt{B_R}$  if  $T > \Delta_R$ . At the quantum critical point  $\lambda = 1$ , it becomes the butterfly velocity  $v_{soc}$  of the slow-Goldstone boson in Eq.(23). Obviously, if one sets  $B = 0$  by mistake, Eq.(14) recovers the second equation in Eq.(11), which is the linear spurious roton mode.

Of course, due to the momentum separation as stressed below Eq.(A7), the superfluid Goldstone mode  $\omega_1(\mathbf{q})$  dictated by the  $U_c(1)$  symmetry breaking remains the same as listed the first equation in Eq.(11).

It is important to stress that the Eq.(14) goes well beyond Eq.(13) in many respects: it not only contains the roton gap  $\Delta_R$  in Eq.(13) at the zero momentum  $q = 0$ , but also the roton dispersion relation at long wavelength due to the non-perturbative effect. This is the first non-perturbative calculation of the correction to the dispersion relation beyond just a gap calculation in [10]. Furthermore, by taking  $\lambda \rightarrow 1^-$  limit in Eq.(14), the roton gap vanishes and recovers the linear dispersion in Eq.(23) for the slow-Goldstone mode. So it is the non-perturbative formalism which leads to both the Lyapunov exponent

$\lambda_{B,R}$ , the butterfly velocity  $v_{B,R}$ , and the associated light cone  $x - v_{B,R}t$  in both the pseudo-Goldstone mode at  $\lambda < 1$  and the slow-Goldstone mode at  $\lambda = 1$ .

## Appendix B: Path integral approach to capture the non-perturbative effect

We perform our non-perturbative analysis in the Z-x representation, though equivalent results may be obtained in the Y-x representation (Fig.2). The path integral approach is complementary to the canonical approach presented in Appendix A.

In the weak interaction limit, the low-energy physics can be captured by phase-amplitude representation of original boson in Eq.(A1):

$$b(\tau) = \sqrt{n(\tau)} e^{i\chi(\tau)} [c_1(\tau)\eta_1 e^{i\mathbf{K}_1 \cdot \mathbf{r}_i} + c_2(\tau)\eta_2 e^{i\mathbf{K}_2 \cdot \mathbf{r}_i}], \quad (\text{B1})$$

where  $c_{1,2}$  are given in the Z-x representation Eq.(6). Here, we focus on the two lowest excitation modes: superfluid (density) mode and the roton (SOC) mode, so we drop the gapped quantum fluctuations in the two spinors  $\eta_{1,2}$  in Eq.(A2).

The Lagrangian density takes the form

$$\begin{aligned} \mathcal{L} &= \sum_k b_k^\dagger \partial_\tau b_k + \mathcal{H}[b, b^\dagger] \\ &\approx \sum_k b_k^\dagger (\partial_\tau + \epsilon_k^- - \mu) b_k - E_{\text{int}}[\{c_i\}], \end{aligned} \quad (\text{B2})$$

where the mean-field interaction energy density takes the form Eq.(7)

$$E_{\text{int}}^0 = \frac{Un^2}{2} \left[ 1 + \frac{\lambda - 1}{2} \sin^2 \theta \right], \quad (\text{B3})$$

which determines  $\theta = \pi/2$  but cannot determine  $\phi$ . However, the OFQD analysis indicates that the PW-X SF is the ground state, which means  $(c_1, c_2) = (1, 0)$  or  $(c_1, c_2) = (0, 1)$ , thus suggests  $\phi = 0$ . Plugging in  $\theta = \pi/2$  gives  $c_1 = \cos(\phi/2)$  and  $c_2 = i \sin(\phi/2)$ .

The quantum ground-state (saddle point solution) corresponds to  $(n, \chi, \theta, \phi) = (n_0, 0, \pi/2, 0)$  and the quantum fluctuations can be written as the deviations around the saddle point solution:  $n = n_0 + \delta n$ ,  $\chi = 0 + \delta \chi$ ,  $\theta = \pi/2 + \delta \theta$ ,  $\phi = 0 + \delta \phi$ . Working out fluctuations in the original Hamiltonian and dropping unimportant constants yields the Lagrangian:

$$\begin{aligned} \mathcal{L} &= i\delta n \partial_\tau \chi + i \frac{n_0}{2} \delta \theta \partial_\tau \delta \phi \\ &+ \frac{1}{4} t n_0 \left[ \frac{1}{n_0^2} (\tilde{\nabla} \delta n)^2 + 4(\tilde{\nabla} \delta \chi)^2 + (\tilde{\nabla} \delta \theta)^2 + (\tilde{\nabla} \delta \phi)^2 \right] \\ &+ \frac{1}{4} U [(1 + \lambda)(\delta n)^2 + (1 - \lambda)n_0^2(\delta \theta)^2], \end{aligned} \quad (\text{B4})$$

where  $\tilde{\nabla} = (\partial_x, \sqrt{\cos \beta - \sin^2 \beta} \partial_y)$ .

Besides, we can expand the quantum ground-state energy as

$$\delta E(c_1, c_2) = \frac{1}{2} B (\delta\phi)^2 \quad (\text{B5})$$

By adding it to the Lagrangian to reach a new Lagrangian, one can solve for its two eigen modes  $(\delta n, \delta\chi)$  and  $(\delta\theta, \delta\phi)$  in the momentum space:

$$\begin{aligned} \omega_1 &= \sqrt{g_{\mathbf{k}}[g_{\mathbf{k}} + (1 + \lambda)n_0 U]}, \\ \omega_2 &= \sqrt{[g_{\mathbf{k}} + (1 - \lambda)n_0 U][g_{\mathbf{k}} + 2B/n_0]}, \end{aligned} \quad (\text{B6})$$

where  $g_{\mathbf{k}} = tk_x^2 + tu(\beta)k_y^2$ . As expected, the superfluid Goldstone mode  $\omega_1$  is independent of the  $B$  term.

The non-perturbative analysis generates a gap  $\Delta_R = \sqrt{2BU(1 - \lambda)}$  for the pseudo-Goldstone mode  $\omega_2$  at  $\mathbf{k} = 0$ , but extends significantly to the full spectrum. Since  $B$  remains finite as  $\lambda \rightarrow 1$ , the roton gap behaves as  $\Delta_R \propto \sqrt{1 - \lambda}$  for  $\lambda < 1$ . Results from both complementary approaches are consistent. Dropping the  $B$  term and taking the long-wave length limit recovers  $\omega_1$  and  $\omega_2$  from Eq. (11).

In fact, one can extract the superfluid and roton mode separately from Eq.(B4) and Eq.(B5), one can integrate out  $\delta n$  and  $\delta\phi$  which are conjugate to  $\delta\chi$  and  $\delta\theta$  in Eq.(B4), and obtain

$$\begin{aligned} \mathcal{L}_{\text{eff}} &= \frac{1}{U(1 + \lambda)} (\partial_\tau \chi)^2 + n_0 t (\tilde{\nabla} \delta\chi)^2 + \frac{n_0^2}{8B} (\partial_\tau \delta\theta)^2 \\ &\quad + \frac{1}{4} n_0 t (\tilde{\nabla} \delta\theta)^2 + \frac{1}{4} (1 - \lambda) n_0^2 U (\delta\theta)^2. \end{aligned} \quad (\text{B7})$$

After taking into account the anisotropy encoded in the derivative  $\tilde{\nabla} = (\partial_x, \sqrt{\cos\beta - \sin^2\beta} \partial_y)$ , one can read out the zero-temperature compressibility and superfluid density from the density channel  $\delta\chi$ :

$$\chi^{\text{SF}} = \frac{1}{U(1 + \lambda)}, \quad \rho_x^{\text{SF}} = n_0 t, \quad \rho_y^{\text{SF}} = n_0 t u(\beta), \quad (\text{B8})$$

and also the extra slow-Goldstone mode at  $\lambda = 1$  from the SOC channel  $\delta\theta$ :

$$\chi^{\text{soc}} = \frac{n_0^2}{8B}, \quad \rho_x^{\text{soc}} = \frac{1}{4} n_0 t, \quad \rho_y^{\text{soc}} = \frac{1}{4} n_0 t u(\beta). \quad (\text{B9})$$

When  $\beta$  is small, the anisotropy becomes small. Note that  $\chi^{\text{soc}} \ll \chi^{\text{SF}}$  leads to the relation  $v_{\text{soc}} = \sqrt{\rho^{\text{SF}}/\chi^{\text{SF}}} \ll c = \sqrt{\rho^{\text{soc}}/\chi^{\text{soc}}}$ .

At low temperatures, the superfluid densities in both sectors decrease. They vanish via universal jumps at critical temperatures:  $T_{\text{KT}}^{\text{SF}}$  for the charge  $U(1)_c$  symmetry breaking and  $T_{\text{KT}}^{\text{soc}}$  for the spin-orbit  $U(1)_{\text{soc}}$  symmetry breaking. Following Landau's approach [11], the superfluid density follows  $\rho_s(T) = \rho_s(0) - \rho_n(T)$ , where the normal density  $\rho_n(T) \propto T^3/v^4$  depends on the velocity:  $v = c$  for the superfluid Goldstone mode and  $v = v_{\text{soc}}$  for the slow-Goldstone mode. The small ratio  $r_G$  between the slow-Goldstone and superfluid Goldstone mode velocities yields the hierarchy  $T_{\text{KT}}^{\text{soc}} \ll T_{\text{KT}}^{\text{SF}}$ , as shown in Fig. 5(a).

### Appendix C: Details on the series expansion Eq.(8)

In order to unify calculations for all  $\lambda$  case, we take the most general state and rewrite the Bose field into a mean-field part plus a fluctuating part

$$\begin{pmatrix} b_{\mathbf{k}\uparrow} \\ b_{\mathbf{k}\downarrow} \end{pmatrix} = \sqrt{N_0} \left[ \frac{c_1}{\sqrt{2}} \begin{pmatrix} 1 \\ -1 \end{pmatrix} \delta_{\mathbf{k}, \mathbf{K}} + \frac{c_2}{\sqrt{2}} \begin{pmatrix} 1 \\ 1 \end{pmatrix} \delta_{\mathbf{k}, -\mathbf{K}} \right] + \begin{pmatrix} \psi_{\mathbf{k}\uparrow} \\ \psi_{\mathbf{k}\downarrow} \end{pmatrix}, \quad (\text{C1})$$

where  $c_1$  and  $c_2$  are two complex numbers subject to the normalization condition  $|c_1|^2 + |c_2|^2 = 1$ , and  $N_0$  is the number of condensate atoms. Performing the above substitution, lead to an expansion of original Hamiltonian

$$\mathcal{H} = \mathcal{H}^{(0)} + \mathcal{H}^{(1)} + \mathcal{H}^{(2)} + \dots, \quad (\text{C2})$$

where the superscript denotes the order in the fluctuations and  $\dots$  means high order. After some algebras, the  $\mathcal{H}^{(0)}$  term takes the form

$$\mathcal{H}^{(0)} = -n_0 [2t(1 + \cos\beta) + \mu] + \frac{Un_0^2}{2} \left( 1 + \frac{\lambda - 1}{2} [1 - (c_1 c_2^* + c_1^* c_2)^2] \right), \quad (\text{C3})$$

and  $\mathcal{H}^{(1)}$  term can be easily worked out

$$\begin{aligned} \mathcal{H}^{(1)} &= \sqrt{\frac{N_0}{2}} \left( [-2t(1 + \cos\beta) - \mu] c_1 + \frac{Un_0}{2} [(1 + \lambda)c_1 + (1 - \lambda)c_2(c_1 c_2^* + c_1^* c_2)] \right) (\psi_{\mathbf{K}\uparrow}^\dagger - \psi_{\mathbf{K}\downarrow}^\dagger) \\ &\quad + \sqrt{\frac{N_0}{2}} \left( [-2t(1 + \cos\beta) - \mu] c_2 + \frac{Un_0}{2} [(1 + \lambda)c_2 + (1 - \lambda)c_1(c_1 c_2^* + c_1^* c_2)] \right) (\psi_{-\mathbf{K}\uparrow}^\dagger + \psi_{-\mathbf{K}\downarrow}^\dagger) + h.c.. \end{aligned} \quad (\text{C4})$$



From  $\mathcal{H}^{(1)} = 0$ , the chemical potential can be determined, along with a constraint on  $c_{1,2}$ :

$$\text{when } \lambda < 1, \quad \mu = -2t(1 + \cos \beta) + Un_0(1 + \lambda)/2, \quad c_1 c_2^* + c_1^* c_2 = 0; \quad (\text{C5})$$

$$\text{when } \lambda = 1, \quad \mu = -2t(1 + \cos \beta) + Un_0, \quad \text{any } c_1 c_2^* + c_1^* c_2; \quad (\text{C6})$$

$$\text{when } \lambda > 1, \quad \mu = -2t(1 + \cos \beta) + Un_0, \quad c_1 c_2^* + c_1^* c_2 = \pm 1; \quad (\text{C7})$$

then  $\mathcal{H}^{(2)}$  term is a quadratic theory

$$\begin{aligned} \mathcal{H}^{(2)} = & \sum_{\mathbf{k}} \psi_{\mathbf{k}}^\dagger h_{\mathbf{k}} \psi_{\mathbf{k}} - \mu \sum_{\mathbf{k}} \psi_{\mathbf{k}}^\dagger \psi_{\mathbf{k}} + \frac{Un_0}{2} \sum_{\mathbf{k}} [(2 + \lambda)(\psi_{\mathbf{k}\uparrow}^\dagger \psi_{\mathbf{k}\uparrow} + \psi_{\mathbf{k}\downarrow}^\dagger \psi_{\mathbf{k}\downarrow}) + \lambda(|c_2|^2 - |c_1|^2)(\psi_{\mathbf{k}\uparrow}^\dagger \psi_{\mathbf{k}\downarrow} + \psi_{\mathbf{k}\downarrow}^\dagger \psi_{\mathbf{k}\uparrow})] \\ & + \frac{Un_0}{4} \sum_{\mathbf{k}} [2c_1 c_2 (\psi_{\mathbf{k}\uparrow}^\dagger \psi_{-\mathbf{k}\uparrow}^\dagger - \psi_{\mathbf{k}\downarrow}^\dagger \psi_{-\mathbf{k}\downarrow}^\dagger) + (c_1^2 + c_2^2)(\psi_{\mathbf{k}\uparrow}^\dagger \psi_{-\mathbf{k}+\mathbf{Q}\uparrow}^\dagger + \psi_{\mathbf{k}\downarrow}^\dagger \psi_{-\mathbf{k}+\mathbf{Q}\downarrow}^\dagger) + 2\lambda(c_2^2 - c_1^2)\psi_{\mathbf{k}\uparrow}^\dagger \psi_{-\mathbf{k}+\mathbf{Q}\downarrow}^\dagger + h.c.] \\ & + \frac{Un_0}{2} \sum_{\mathbf{k}} [(2 - \lambda)(c_1 c_2^* + c_1^* c_2)(\psi_{\mathbf{k}\uparrow}^\dagger \psi_{\mathbf{k}+\mathbf{Q}\uparrow}^\dagger - \psi_{\mathbf{k}\downarrow}^\dagger \psi_{\mathbf{k}+\mathbf{Q}\downarrow}^\dagger) + \lambda(c_1 c_2^* - c_1^* c_2)(\psi_{\mathbf{k}\uparrow}^\dagger \psi_{\mathbf{k}+\mathbf{Q}\downarrow}^\dagger - \psi_{\mathbf{k}\downarrow}^\dagger \psi_{\mathbf{k}+\mathbf{Q}\uparrow}^\dagger)], \end{aligned} \quad (\text{C8})$$

where we define  $\mathbf{Q} = 2\mathbf{K} = (\pi, 0)$ . To incorporate both spin and valley degrees of freedom, a spinor is introduced as:  $\Psi_{\mathbf{k}} = (\psi_{\mathbf{K}+\mathbf{k},\uparrow}, \psi_{\mathbf{K}+\mathbf{k},\downarrow}, \psi_{-\mathbf{K}+\mathbf{k},\uparrow}, \psi_{-\mathbf{K}+\mathbf{k},\downarrow})^\top$ . In this notation, the Hamiltonian  $\mathcal{H}^{(2)}$  can be expressed in matrix form as

$$\mathcal{H}^{(2)} = \frac{1}{2} \sum_{\mathbf{k} \in \text{RBZ}} \text{Tr} M_{22}(\mathbf{k}) + \frac{1}{2} \sum_{\mathbf{k} \in \text{RBZ}} \begin{pmatrix} \Psi_{\mathbf{k}}^\dagger & \Psi_{-\mathbf{k}}^\top \end{pmatrix} \begin{pmatrix} M_{11}(\mathbf{k}) & M_{12}(\mathbf{k}) \\ M_{21}(\mathbf{k}) & M_{22}(\mathbf{k}) \end{pmatrix} \begin{pmatrix} \Psi_{\mathbf{k}} \\ \Psi_{-\mathbf{k}}^\top \end{pmatrix}, \quad (\text{C9})$$

where  $M_{ij}$  for  $i, j = 1, 2$  are  $4 \times 4$  matrix, and the overall  $8 \times 8$  matrix is referred to as  $M$ . Note the off-block-diagonal part  $M_{12}$  and  $M_{21}$  are comes from anomalous terms in Eq.(C8). The bosonic commutation relation and Hermiticity yield the relationships  $M_{11}(\mathbf{k}) = M_{22}(-\mathbf{k})^\top$  and  $M_{12}(\mathbf{k}) = [M_{21}(\mathbf{k})]^\dagger$ . It is convenient to decompose  $M$  into three parts:  $M = M^{(t)} + M^{(\mu)} + M^{(U)}$ , where  $M_{ij}^{(\mu)} = \mu \delta_{ij} I_{4 \times 4}$ ,  $M_{12}^{(t)} = M_{21}^{(t)} = 0$  and

$$M_{11}^{(t)}(\mathbf{k}) = -2t \begin{pmatrix} \cos \beta \cos k_y & -\cos k_x + i \sin \beta \sin k_y & 0 & 0 \\ -\cos k_x - i \sin \beta \sin k_y & \cos \beta \cos k_y & 0 & 0 \\ 0 & 0 & \cos \beta \cos k_y & \cos k_x + i \sin \beta \sin k_y \\ 0 & 0 & \cos k_x - i \sin \beta \sin k_y & \cos \beta \cos k_y \end{pmatrix}, \quad (\text{C10})$$

and the block-diagonal part of  $M^{(U)}$

$$M_{11}^{(U)}(\mathbf{k}) = Un_0 \begin{pmatrix} 1 + \lambda/2 & (\lambda/2)(|c_2|^2 - |c_1|^2) & (1 - \lambda/2)(c_1 c_2^* + c_1^* c_2) & (\lambda/2)(c_1 c_2^* - c_1^* c_2) \\ (\lambda/2)(|c_2|^2 - |c_1|^2) & 1 + \lambda/2 & \lambda/2(c_1^* c_2 - c_1 c_2^*) & (\lambda/2 - 1)(c_1 c_2^* + c_1^* c_2) \\ (1 - \lambda)(c_1 c_2^* + c_1^* c_2) & (\lambda/2)(c_1 c_2^* - c_1^* c_2) & 1 + \lambda/2 & (\lambda/2)(|c_2|^2 - |c_1|^2) \\ (\lambda/2)(c_1^* c_2 - c_1 c_2^*) & (\lambda/2 - 1)(c_1 c_2^* + c_1^* c_2) & (\lambda/2)(|c_2|^2 - |c_1|^2) & 1 + \lambda/2 \end{pmatrix}, \quad (\text{C11})$$

as well as off-block-diagonal part of  $M^{(U)}$

$$M_{12}^{(U)}(k) = Un_0 \begin{pmatrix} (c_1^2 + c_2^2)/2 & (\lambda/2)(c_2^2 - c_1^2) & c_1 c_2 & 0 \\ (\lambda/2)(c_2^2 - c_1^2) & (c_1^2 + c_2^2)/2 & 0 & -c_1 c_2 \\ c_1 c_2 & 0 & (c_1^2 + c_2^2)/2 & (\lambda/2)(c_2^2 - c_1^2) \\ 0 & -c_1 c_2 & (\lambda/2)(c_2^2 - c_1^2) & (c_1^2 + c_2^2)/2 \end{pmatrix}. \quad (\text{C12})$$

It is well known that Hamiltonian Eq.(C9) can be diagonalized by a  $8 \times 8$  Bogoliubov transformation

$$\mathcal{H}^{(2)} = \frac{1}{2} \sum_{\mathbf{k} \in \text{RBZ}} \text{Tr} M_{22}(\mathbf{k}) + \frac{1}{2} \sum_{\mathbf{k} \in \text{RBZ}} \begin{pmatrix} \beta_{\mathbf{k}}^\dagger & \beta_{-\mathbf{k}}^\top \end{pmatrix} \begin{pmatrix} \Omega(\mathbf{k}) & 0 \\ 0 & \Omega(-\mathbf{k}) \end{pmatrix} \begin{pmatrix} \beta_{\mathbf{k}} \\ \beta_{-\mathbf{k}}^\top \end{pmatrix} \quad (\text{C13})$$

$$\beta_{\mathbf{k}} = \mathbf{u}_{\mathbf{k}} \Psi_{\mathbf{k}} + \mathbf{v}_{-\mathbf{k}} \Psi_{-\mathbf{k}}^\dagger, \quad \beta_{-\mathbf{k}}^\dagger = \mathbf{u}_{-\mathbf{k}}^* \Psi_{-\mathbf{k}}^\dagger + \mathbf{v}_{\mathbf{k}}^* \Psi_{\mathbf{k}}, \quad (\text{C14})$$

where  $\Omega(\mathbf{k}) = \text{diag}(\omega_{1,\mathbf{k}}, \omega_{2,\mathbf{k}}, \omega_{3,\mathbf{k}}, \omega_{4,\mathbf{k}})$ ,  $\beta_{\mathbf{k}} = (\beta_{1,\mathbf{k}}, \beta_{2,\mathbf{k}}, \beta_{3,\mathbf{k}}, \beta_{4,\mathbf{k}})$  and  $\mathbf{u}_{\mathbf{k}}, \mathbf{v}_{\mathbf{k}}$  are two  $4 \times 4$  matrix. To ensure the Bogoliubov transformation is canonical,  $\beta_{l,\mathbf{k}}$  must satisfy bosonic commutation relation, i.e.  $[\beta_{l,\mathbf{k}}, \beta_{l',\mathbf{k}'}^\dagger] = \delta_{l,l'} \delta_{\mathbf{k},\mathbf{k}'}$ , and  $[\beta_{l,\mathbf{k}}, \beta_{l',\mathbf{k}'}] = 0$ . These conditions will give constraint to  $\mathbf{u}_{\mathbf{k}}$  and  $\mathbf{v}_{\mathbf{k}}$ , which results in a secular equation

$$\det \begin{pmatrix} M_{11}(\mathbf{k}) - \omega_{l,\mathbf{k}} I & M_{12}(\mathbf{k}) \\ M_{21}(\mathbf{k}) & M_{22}(\mathbf{k}) + \omega_{l,\mathbf{k}} I \end{pmatrix} = 0 \quad (\text{C15})$$

where  $I$  stand for a  $4 \times 4$  identity matrix, and  $\omega_l$  are eigen-energy after Bogoliubov transformation.

After combined condition Eq.(C5-C7) and the secular equation Eq.(C15) and then solve it, we accomplished the diagonalization of the quadratic theory

$$\mathcal{H}^{(2)} = E_0^{(2)} + \sum_{\mathbf{k}} \sum_{l=1}^4 \omega_{l,\mathbf{k}} \left( \beta_{l,\mathbf{k}}^\dagger \beta_{l,\mathbf{k}} + \frac{1}{2} \right) \quad (\text{C16})$$

In general, it is challenging to diagonalize the matrix analytically; however, numerical methods can always be employed to extract useful information.

#### Appendix D: Details on the evaluation of the velocity ratio $v_{\text{soc}}/c$

This section provides technical details on the evaluation of the velocity of the slow-Goldstone mode. The following calculations are performed under the condition  $\lambda \leq 1$ , and the parameterization of  $c_1$  and  $c_2$  from Eq.(6) is used.

For generic  $\phi$ , the 4 Bogoliubov bands  $\omega_l(\mathbf{k}; \phi)$  in Eq. (C16) are quite complicated, but they simplify considerably at  $\phi = 0$  as:

$$\begin{aligned} \omega_1(\mathbf{k}; \phi = 0) &= \sqrt{A_1 + \sqrt{A_1^2 - B_1^2}}, & \omega_2(\mathbf{k}; \phi = 0) &= \sqrt{A_1 - \sqrt{A_1^2 - B_1^2}}, \\ \omega_3(\mathbf{k}; \phi = 0) &= \sqrt{A_2 + \sqrt{A_2^2 - B_2^2}}, & \omega_4(\mathbf{k}; \phi = 0) &= \sqrt{A_2 - \sqrt{A_2^2 - B_2^2}}, \end{aligned} \quad (\text{D1})$$

where we define

$$\begin{aligned} A_s &= h_0(h_0 + n_0 U) + h_x^2 + h_y^2 + (-1)^s n_0 U \lambda h_x, \\ B_s^2 &= (h_0^2 - h_x^2 - h_y^2)[h_0^2 - h_x^2 - h_y^2 + n_0 U(2h_0 - 2\lambda h_x + (1 - \lambda^2)n_0 U)], \\ h_0 &= 2t(1 + \cos \beta) - 2t \cos \beta \cos k_y, \quad h_x = 2t \cos k_x, \quad h_y = -i2t \sin \beta \sin k_y. \end{aligned} \quad (\text{D2})$$

However, the secular equation of arbitrary  $\phi$  can be significantly simplified using the results obtained at  $\phi = 0$ :

$$0 = (\omega^2 - \omega_1^2)(\omega^2 - \omega_2^2)(\omega^2 - \omega_3^2)(\omega^2 - \omega_4^2) - f, \quad (\text{D3})$$

where  $\omega_i = \omega_i(\mathbf{k}; \phi = 0)$  and  $f = f(\omega, \phi)$  with  $f(\omega, \phi = 0) = 0$ . Nevertheless, it is generally an eighth-degree equation, and there is no analytical method to obtain an exact solution, although numerical methods are always available.

The ground-state energy  $E_{\text{GS}}(\phi)$  in Eq. (10) is

$$E_{\text{GS}}(\phi) = E_{0t} + \frac{1}{2} \sum_{l,\mathbf{k}} \omega_l(\mathbf{k}; \phi), \quad (\text{D4})$$

which is plotted as a function of  $\phi$  for various  $\lambda$  in Fig.3(a). The numerical data of  $E_{\text{GS}}(\phi)$  shows minima at  $\phi = 0$  and  $\phi = \pi$ . In order to evaluate  $B$  analytically, one need take derivative with respect to  $\phi$  at  $\phi = 0, \pi$

$$B(n_0 U, t, \beta, \lambda) = \frac{\partial^2}{\partial \phi^2} \Big|_{\phi=0} \frac{1}{2} \sum_{\mathbf{k} \in \text{RBZ}} \sum_{l=1}^4 \omega_l(\mathbf{k}; \phi). \quad (\text{D5})$$

Thus derivative of  $\omega_l(\mathbf{k}; \phi)$  with respect to  $\phi$  is crucial in determining  $B$ . The perturbative approach to solving the general secular equation Eq.(D3) yields these derivatives. Thus, the exact analytical expression of  $B$  is obtained as

$$\begin{aligned} B(n_0 U, t, \beta, \lambda) &= \sum_{\mathbf{k}} \frac{g_1(\omega_1 + \omega_2 + \omega_3 + \omega_4)}{(\omega_1 + \omega_2)(\omega_1 + \omega_3)(\omega_1 + \omega_4)(\omega_2 + \omega_3)(\omega_2 + \omega_4)(\omega_3 + \omega_4)} \\ &+ \sum_{\mathbf{k}} \frac{g_2(\omega_1 \omega_2 \omega_3 + \omega_1 \omega_2 \omega_4 + \omega_1 \omega_3 \omega_4 + \omega_2 \omega_3 \omega_4)}{(\omega_1 + \omega_2)(\omega_1 + \omega_3)(\omega_1 + \omega_4)(\omega_2 + \omega_3)(\omega_2 + \omega_4)(\omega_3 + \omega_4)} \\ &+ \sum_{\mathbf{k}} \frac{g_3[(\omega_1 + \omega_2 + \omega_3 + \omega_4)^3 - \omega_1^3 - \omega_2^3 - \omega_3^3 - \omega_4^3]}{3\omega_1 \omega_2 \omega_3 \omega_4 (\omega_1 + \omega_2)(\omega_1 + \omega_3)(\omega_1 + \omega_4)(\omega_2 + \omega_3)(\omega_2 + \omega_4)(\omega_3 + \omega_4)}, \end{aligned} \quad (\text{D6})$$

where  $\omega_l \equiv \omega_l(k; \phi = 0)$  are listed in Eq.(D2) and

$$g_1 = 16n_0^2 U^2 h_0^2 h_y^2 - 4(1 - \lambda^2)n_0^2 U^2 h_y^2 (3h_0^2 - h_x^2 - h_y^2 + n_0 U h_0), \quad (D7)$$

$$g_2 = 2(1 - \lambda^2)n_0^2 U^2 h_y^2, \quad (D8)$$

$$g_3 = 2(1 - \lambda^2)n_0^2 U^2 h_y^2 (h_0^2 - h_x^2 - h_y^2) [h_0^2 - h_x^2 - h_y^2 + 2n_0 U h_0 + (1 - \lambda^2)n_0^2 U^2]. \quad (D9)$$

At  $\lambda = 1$ ,  $B$  takes the simpler form:

$$B(n_0 U, t, \beta, \lambda = 1) = \sum_{\mathbf{k}} \frac{16n_0^2 U^2 h_0^2 h_y^2 (\omega_1 + \omega_2 + \omega_3 + \omega_4)}{(\omega_1 + \omega_2)(\omega_1 + \omega_3)(\omega_1 + \omega_4)(\omega_2 + \omega_3)(\omega_2 + \omega_4)(\omega_3 + \omega_4)}. \quad (D10)$$

It is easy to scale out the overall factor  $(n_0 U \sin \beta)^2 / t$  and rewrite  $B = b(n_0 U \sin \beta)^2 / t$  with a dimensionless quantity  $b$ . The limiting value of  $b$  as  $\beta \rightarrow 0$  and  $U \rightarrow 0$  can be analytical worked out as

$$\lim_{\beta \rightarrow 0} \lim_{U \rightarrow 0} b = \lim_{\beta \rightarrow 0} \lim_{U \rightarrow 0} \frac{B(\lambda = 1)}{(n_0 U \sin \beta)^2 / t} = \frac{3 - \sqrt{3} \ln(2 + \sqrt{3})}{12\pi} \approx 0.01907. \quad (D11)$$

The  $B$  and  $b$  are plotted as a function of  $n_0 U / t$  for various  $\beta$  in Fig.3(b). At  $\lambda = 1$ , the ratio between the slope of slow-Goldstone mode and that of the superfluid Goldstone mode is given by

$$r_G = \frac{\sqrt{2Bt/n_0}}{\sqrt{2n_0 t U}} = \sqrt{\frac{B}{n_0^2 U}} = \sqrt{\frac{b(n_0 U)^2 \sin^2 \beta / t}{n_0^2 U}} = \sqrt{b(U/t) \sin^2 \beta}. \quad (D12)$$

The typical value for  $r_G$  is  $\approx 1\%$  shown in Fig.5(b).

- 
- [1] M. E. Peskin and D. V. Schroeder, *Quantum Field Theory*, (1st edition, Westview Press 1995).
  - [2] David Sauzin, Introduction to 1-summability and resurgence, arXiv:1405.0356
  - [3] M. Mariño, Lectures on non-perturbative effects in large N gauge theories, matrix models and strings, Fortsch. Phys. **62**, 455 (2014).
  - [4] Inês Aniceto, Gökçe Başar, Ricardo Schiappa, A primer on resurgent transseries and their asymptotics, Physics Reports **809**, 1 (2019).
  - [5] S. Sachdev and J. Ye, Universal quantum-critical dynamics of two-dimensional antiferromagnets, Phys. Rev. Lett. **69**, 2411 (1992).
  - [6] S. Sachdev, *Quantum Phase transitions*, (2nd edition, Cambridge University Press, 2011).
  - [7] S. Sachdev and J. Ye, Gapless spin-fluid ground state in a random quantum Heisenberg magnet, Phys. Rev. Lett. **70**, 3339 (1993).
  - [8] A. Kitaev, A simple model of quantum holography, KITP strings seminar and Entanglement 2015 program (Feb. 12, April 7, and May 27, 2015) . <http://online.kitp.ucsb.edu/online/entangled15/>.
  - [9] J. Maldacena and D. Stanford, Remarks on the Sachdev-Ye-Kitaev model, Phys. Rev. D **94**, 106002 (2016).
  - [10] Murthy, G., Arovas, D. & Auerbach, A. Superfluids and supersolids on frustrated two-dimensional lattices. Phys. Rev. B **55**, 3104 (1997).
  - [11] For a review, see A. L. Fetter and J. D. Walecka, *Quantum Theory of many-particle Systems*, Dover Publications, Inc. Mineola, New York, 2002.
  - [12] Wang Yao and Qian Niu, Berry Phase Effect on the Exciton Transport and on the Exciton Bose-Einstein Condensate, Phys. Rev. Lett. **101**, 106401 (2008).
  - [13] Naoto Nagaosa, Jairo Sinova, Shigeki Onoda, A. H. MacDonald, and N. P. Ong, Anomalous Hall effect, Rev. Mod. Phys. **82**, 1539 (2010).
  - [14] Y. A. Bychkov and E.I. Rashba, Oscillatory effects and the magnetic susceptibility of carriers in inversion layers, J. Phys. C: Solid State Phys. **17**, 6039 (1984).
  - [15] T. Jungwirth, Qian Niu and A. H. MacDonald, Anomalous Hall Effect in Ferromagnetic Semiconductors, Phys. Rev. Lett. **88**, 207208 (2004).
  - [16] Jinwu Ye, Yong Baek Kim, A. J. Millis, B. I. Shraiman, P. Majumdar, and Z. Tesanovic, Berry phase theory of the Anomalous Hall Effect: Application to Colossal Magnetoresistance Manganites, Phys. Rev. Lett. **83**, 3737 (1999).
  - [17] Lev P. Gor'kov and Emmanuel I. Rashba, Superconducting 2D System with Lifted Spin Degeneracy: Mixed Singlet-Triplet State, Phys. Rev. Lett. **87**, 037004 (2001).
  - [18] Lianghui Huang, Zengming Meng, Pengjun Wang, Peng Peng, Shao-Liang Zhang, Liangchao Chen, Donghao Li, Qi Zhou & Jing Zhang Experimental realization of a two-dimensional synthetic spin-orbit coupling in ultracold Fermi gases, Nature Physics **12**, 540 (2016). However, the heating is still serious which prevents the observation of many body phenomena due to the Rashba SOC for the alkali atoms. So the physics observed in [18, 19] is still at single particle physics.
  - [19] Zengming Meng, Lianghui Huang, Peng Peng, Donghao

- Li, Liangchao Chen, Yong Xu, Chuanwei Zhang, Pengjun Wang, Jing Zhang, Experimental observation of topological band gap opening in ultracold Fermi gases with two-dimensional spin-orbit coupling, *Phys. Rev. Lett.* 117, 235304 (2016).
- [20] Zhan Wu, Long Zhang, Wei Sun, Xiao-Tian Xu, Bao-Zong Wang, Si-Cong Ji, Youjin Deng, Shuai Chen, Xiong-Jun Liu, Jian-Wei Pan, Realization of Two-Dimensional Spin-orbit Coupling for Bose-Einstein Condensates, *Science* 354, 83-88 (2016). Indeed, the lifetime of SOC  $^{87}\text{Rb}$  BEC was already made as long as 300ms in this work and improved to  $\sim 1\text{s}$  recently, so the current experiment set-up the stage to observe any possible many body phenomena at a weak interaction where the heating rate is well under control.
- [21] O. Boada, A. Celi, J. I. Latorre, and M. Lewenstein, Quantum Simulation of an Extra Dimension, *Phys. Rev. Lett.* 108, 133001 (2012);
- [22] A. Celi, P. Massignan, J. Ruseckas, N. Goldman, I. Spielman, G. Juzeliūnas, and M. Lewenstein Synthetic Gauge Fields in Synthetic Dimensions, *Phys. Rev. Lett.* 112, 043001 (2014).
- [23] Michael L. Wall, Andrew P. Koller, Shuming Li, Xibo Zhang, Nigel R. Cooper, Jun Ye, Ana Maria Rey, Synthetic Spin-Orbit Coupling in an Optical Lattice Clock, *Phys. Rev. Lett.* 116, 035301 (2016).
- [24] L. F. Livi, G. Cappellini, M. Diem, L. Franchi, C. Clivati, M. Frittelli, F. Levi, D. Calonico, J. Catani, M. Inguscio, L. Fallani, Synthetic dimensions and spin-orbit coupling with an optical clock transition, *Phys. Rev. Lett.* 117, 220401 (2016).
- [25] S. Kolkowitz, S.L. Bromley, T. Bothwell, M.L. Wall, G.E. Marti, A.P. Koller, X. Zhang, A.M. Rey, J. Ye, Spin-orbit coupled fermions in an optical lattice clock, *Nature* 542, 66 (2017).
- [26] Fangzhao Alex An, Eric J. Meier, Bryce Gadway, Direct observation of chiral currents and magnetic reflection in atomic flux lattices, arXiv:1609.09467.
- [27] Nathaniel Q. Burdick, Yijun Tang, and Benjamin L. Lev, Long-Lived Spin-Orbit-Coupled Degenerate Dipolar Fermi Gas, *Phys. Rev. X* 6, 031022 (2016).
- [28] Fadi Sun, Jinwu Ye, Wu-Ming Liu, Quantum magnetism of spinor bosons in optical lattices with synthetic non-Abelian gauge fields, *Phys. Rev. A* 92, 043609 (2015).
- [29] Here we still use the same notation used in [28]. The PW-X means the plane wave state with the spin polarization along the X direction. The PW-XY means the plane wave state with the spin polarization along the XY direction. In the Z-x phase, the first Capital letter indicates the spin polarization, the second small letter indicates the orbital order.
- [30] Because the bosons can condense at one of the  $N_K = 2$  minima in Fig.1b. In the following, the momentum is measured relative to this condensation point.
- [31] In this manuscript, we use the roton or pseudo-Goldstone mode interchangeably.
- [32] For  $\beta > \beta_c$ , the two minima split into four minima at incommensurate momenta ( $\pm\pi/2, \pm k_0$ ). The physics of this  $N_K = 4$  phase when  $\beta_c < \beta < \pi/2$ , including the quantum Lifshitz transition at  $\beta = \beta_c$  induced by the superfluid Goldstone boson, will be discussed in a separate publication.
- [33] D. van Oosten, P. van der Straten, and H. T. C. Stoof, Quantum phases in an optical lattice, *Phys. Rev. A* 63, 053601 (2001).
- [34] Elliott H. Lieb and Derek W. Robinson, The finite group velocity of quantum spin systems, *Commun. Math. Phys.* 28, 251 (1972).
- [35] C. J. Kennedy, G. A. Siviloglou, H. Miyake, W. C. Burton, and W. Ketterle, Spin-Orbit Coupling and Quantum Spin Hall Effect for Neutral Atoms without Spin Flips, *Phys. Rev. Lett.* 111, 225301 (2013).
- [36] Immanuel Bloch, Jean Dalibard, and Wilhelm Zwerger, Many-body physics with ultracold gases, *Rev. Mod. Phys.* 80, 885 (2008).
- [37] M. Kozuma, *et.al*, Coherent Splitting of Bose-Einstein Condensed Atoms with Optically Induced Bragg Diffraction, *Phys. Rev. Lett.* 82, 871 (1999).
- [38] J. Stenger, *et al*, Bragg Spectroscopy of a Bose-Einstein Condensate, *Phys. Rev. Lett.* 82, 4569 (1999).
- [39] D. M. Stamper-Kurn *et al*, Excitation of Phonons in a Bose-Einstein Condensate by Light Scattering, *Phys. Rev. Lett.* 83, 2876 (1999).
- [40] J. Steinhauer, *et.al*, Excitation Spectrum of a Bose-Einstein Condensate, *Phys. Rev. Lett.* 88, 120407 (2002).
- [41] S. B. Papp, *et.al*, Bragg Spectroscopy of a Strongly Interacting  $^{85}\text{Rb}$  Bose-Einstein Condensate, *Phys. Rev. Lett.* 101, 135301 (2008).
- [42] Kinast, J. *et al*. Heat Capacity of a Strongly Interacting Fermi Gas. *Science* **307**, 1296 (2005).
- [43] Ku, M. J. H. *et al*. Revealing the Superfluid Lambda Transition in the Universal Thermodynamics of a Unitary Fermi Gas. *Science* **335**, 563 (2012).
- [44] Gemelke, N., Zhang X., Huang C. L., and Chin, C. In situ observation of incompressible Mott-insulating domains in ultracold atomic gases, *Nature (London)* **460**, 995 (2009).
- [45] Marc Cheneau, Peter Barmettler, Dario Poletti, Manuel Endres, Peter Schau?, Takeshi Fukuhara, Christian Gross, Immanuel Bloch, Corinna Kollath & Stefan Kuhr, Light-cone-like spreading of correlations in a quantum many-body system, *Nature* 481, 484 (2012)
- [46] Martin Grttner, Justin G. Bohnet, Arghavan Safavi-Naini, Michael L. Wall, John J. Bollinger & Ana Maria Rey, Measuring out-of-time-order correlations and multiple quantum spectra in a trapped-ion quantum magnet. *Nature Physics* 13, 781 (2017).
- [47] For a review, See Jacob B. Khurgin, Slow light in various media: a tutorial, *Advances in Optics and Photonics*, Vol. 2, Issue 3, pp. 287-318 (2010).
- [48] Debanjan Chowdhury, Brian Swingle, Onset of many-body chaos in the O(N) model, *Phys. Rev. D* 96, 065005 (2017).
- [49] S. Coleman and E. Weinberg, Radiative corrections as the origin of spontaneous symmetry breaking, *Phys. Rev. D* 7, 1888 (1973).
- [50] Qian Liang, Zhaoli Dong, Jian-Song Pan, Hongru Wang, Hang Li, Zhaoju Yang, Wei Yi & Bo Yan, Chiral dynamics of ultracold atoms under a tunable SU(2) synthetic gauge field, *Nature Physics* 20, 1738 (2024) .